

1 **Exploring macroevolutionary links in multi-species planktonic foraminiferal Mg/Ca and**
2 **$\delta^{18}\text{O}$ from 15 Ma to Recent**

3 Flavia Boscolo-Galazzo^{1*}, David Evans², Elaine M. Mawbey³, William R. Gray⁴, Paul N.
4 Pearson^{3,5}, Bridget S. Wade³

5 ¹Bremen University, MARUM, Center for Marine Environmental Sciences (Germany);

6 ²School of Ocean and Earth Science, University of Southampton, European Way, SO14 3ZH, Southampton (UK);

7 ³Department of Earth Sciences, University College London, London (UK);

8 ⁴Laboratoire des Sciences du Climat et de l'Environnement (LSCE/IPSL), Université Paris-Saclay, Gif-sur-Yvette (France).

9 ⁵School of Earth and Environmental Sciences, Cardiff University, Cardiff (UK)

10 *Corresponding author: Flavia@uni-bremen.de,

11 d.evans@soton.ac.uk, mawbeye@gmail.com, william.gray@lsce.ipsl.fr, p.pearson@ucl.ac.uk,

12 b.wade@ucl.ac.uk

13 **Abstract**

14 The ratio of the trace element Mg over Ca (Mg/Ca) and the oxygen isotopic composition ($\delta^{18}\text{O}$) of
15 foraminiferal calcite are widely employed for reconstructing past ocean temperatures, although
16 geochemical signals are also influenced by several other factors that vary temporally and spatially.
17 Here, we analyze a global dataset of Mg/Ca and $\delta^{18}\text{O}$ data of 59 middle Miocene to Holocene
18 species of planktonic foraminifera from a wide range of depth habitats, many of which have never
19 been analyzed before for Mg/Ca. We investigate the extent to which Mg/Ca and $\delta^{18}\text{O}$ covary
20 through time and space, and identify several sources of mismatch between the two proxies. Once
21 the data are adjusted for long term non-thermal factors, Mg/Ca and $\delta^{18}\text{O}$ are overall positively
22 correlated in a way consistent with temperature being the dominant controller both through space
23 and time and across many different species, including deep-dwellers. However, we identify several
24 species with systematic offsets in Mg/Ca values, to which multispecies calibrations should be
25 applied with caution. We can track the appearance of such offsets through ancestor-descendent
26 species over the last 15 million years and propose that the emergence of these offsets may be the

27 geochemical expression of evolutionary innovations. We find virtually all of the Mg/Ca and $\delta^{18}\text{O}$ -
28 derived temperatures from the commonly used genera *Globigerinoides* and *Trilobatus* are within
29 uncertainty of each other, highlighting the utility of these species for paleoceanographic
30 reconstructions. Our results highlight the potential of leveraging information from species lineages
31 to improve sea surface temperature reconstruction from planktonic foraminifera over the
32 Cenozoic.

33 **1. Introduction**

34 Geochemical analyses of foraminifera are commonly applied to reconstruct paleoceanographic
35 conditions, such as marine temperatures, and therefore infer past climatic changes. In particular,
36 the fossil tests of planktonic foraminifera (calcareous zooplankton) provide one of the most widely
37 used paleoclimate archives. Here we focus on two of these parameters: $\delta^{18}\text{O}$ and Mg/Ca, both of
38 which have been used widely as temperature proxies.

39 The oldest and possibly most widely utilized of these proxies is the ratio of oxygen isotopes in
40 their calcite test which, due to slight differences in reactivity of molecules containing the different
41 isotopes, is temperature-dependent (Urey, 1947; see Pearson, 2012 for review). This effect has
42 been quantified in experiments with inorganic calcite (e.g., Kim and O'Neill, 1997) and planktonic
43 foraminifera in culture (e.g., Erez and Luz, 1983; Bemis et al., 1998). Tests of planktonic
44 foraminifera calcifying in warmer waters are depleted in ^{18}O relative to species living in cooler
45 waters (Emiliani, 1954). A second, more recently established paleoclimate proxy is the ratio of
46 magnesium to calcium in test calcite (Chave 1954; Nürnberg et al., 1996). During inorganic
47 precipitation experiments, the Mg/Ca ratios of calcite were found to be higher at greater
48 temperatures (Mucci, 1987). This relationship led to the in-depth exploration of Mg/Ca ratios in

49 planktonic and benthic foraminifera and its potential application as a temperature proxy through
50 culturing (Lea et al., 1999; von Langen et al., 2005), core top (Nürnberg, 1995; Elderfield and
51 Gassen, 2000) and sediment trap studies (Anand et al., 2003).

52 As they represent two different chemical systems, the Mg/Ca and oxygen stable isotope ratios in
53 foraminifera are often used together as independent temperature proxies. For instance, $\delta^{18}\text{O}$
54 derived calcification temperatures have been combined with Mg/Ca data to derive Mg/Ca
55 temperature calibrations (e.g., Anand et al., 2003; McConnel and Thunell, 2005; Mohtadi et al.,
56 2009). Other studies have applied these two systems together to infer the influence of
57 environmental parameters such as seawater salinity on Mg/Ca (e.g., Mathien-Blard and Bassinot,
58 2009; Hönisch et al., 2013) and global ice volume (e.g., Lear et al., 2000; Katz et al., 2008). Works
59 such as these assume covariance of the two proxies for any given sample, which should be the case
60 if both systems are impacted purely by calcification temperature. Nonetheless, there are known
61 non-thermal effects influencing both Mg/Ca and $\delta^{18}\text{O}$. For oxygen isotope values, these include
62 the oxygen isotopic composition of seawater ($\delta^{18}\text{O}_{\text{sw}}$) and to a lesser degree, seawater pH or
63 carbonate ion concentration (Spero et al., 1997; Zeebe, 1999). Seawater carbonate chemistry has
64 also been shown to impact the Mg/Ca proxy. Culture and sediment trap studies demonstrate surface
65 ocean seawater pH can influence Mg/Ca in planktonic foraminifera (Lea et al 1999; Evans et al.,
66 2016a; Gray et al 2018), with the sensitivity of Mg/Ca to pH appearing to vary between species
67 (Gray and Evans 2019). Mg/Ca values of foraminifera are also dependent on the Mg/Ca of
68 seawater (Evans et al., 2016b), and both oxygen isotope and Mg/Ca values can be impacted by test
69 recrystallization (Dekens et al., 2002). Mg/Ca values are susceptible to the preferential loss of Mg
70 during dissolution, and are thus influenced by the calcite saturation state of bottom waters
71 (Regenberg et al 2014; Tierney et al 2019). Seawater salinity has a minor secondary effect on

72 Mg/Ca values (Kisakürek et al., 2008, Hönisch et al., 2013) and whilst salinity has little direct
73 effect on oxygen isotopes, a change in salinity is usually accompanied by a change in $\delta^{18}\text{O}_{\text{sw}}$
74 because hydrological processes such as evaporation and precipitation are closely coupled
75 (LeGrande and Schmidt 2006). Lastly, so-called ‘vital effects’, which lump together a wide variety
76 of species-specific processes such as metabolism (including the process of calcification and the
77 incorporation of metabolic products), the position within the water column and life cycle depth
78 migration, the presence of photosymbionts, and seasonality (see summary in Schiebel and
79 Hemleben, 2017), also add complexity to the interpretation of both the oxygen isotope and Mg/Ca
80 proxies.

81 Here we use the dataset published in Boscolo-Galazzo, Crichton et al., (2021), to examine
82 covariance between Mg/Ca and $\delta^{18}\text{O}$ in planktonic foraminifera extracted from sediments across
83 a wide range of geographic locations, time intervals, and species. The dataset is composed of $\delta^{18}\text{O}$
84 and Mg/Ca data measured on 59 species of planktonic foraminifera, of which 24 have never before
85 been measured for Mg/Ca (Supplementary Tables 1, 2). The data are from different ocean basins
86 and latitudes and a range of ages between the middle Miocene (~15 million years ago, Ma) and
87 the Holocene. Paired Mg/Ca and $\delta^{18}\text{O}$ were measured on the same samples, hence this dataset is
88 ideally suited to isolate potential ecological, environmental and preservational factors which may
89 imprint Mg/Ca or $\delta^{18}\text{O}$ or both, and which are otherwise impossible to recognize in studies
90 focusing on a limited number of species, a narrow study area or time interval. In particular, it
91 provides the unique opportunity to simultaneously: (1) compare coupled $\delta^{18}\text{O}$ and Mg/Ca data on
92 a broader than usual geographical and temporal scale; (2) Compare coupled $\delta^{18}\text{O}$ and Mg/Ca data
93 across species of different ecologies; (3) Evaluate Mg/Ca data of extinct species against those of
94 their modern descendants; (4) Test whether temperature can still be recognized as predominantly

95 driving covariance in the dataset when spatial, temporal and ecological variables are
96 simultaneously in play.

97 **2. Material and Analytical methods**

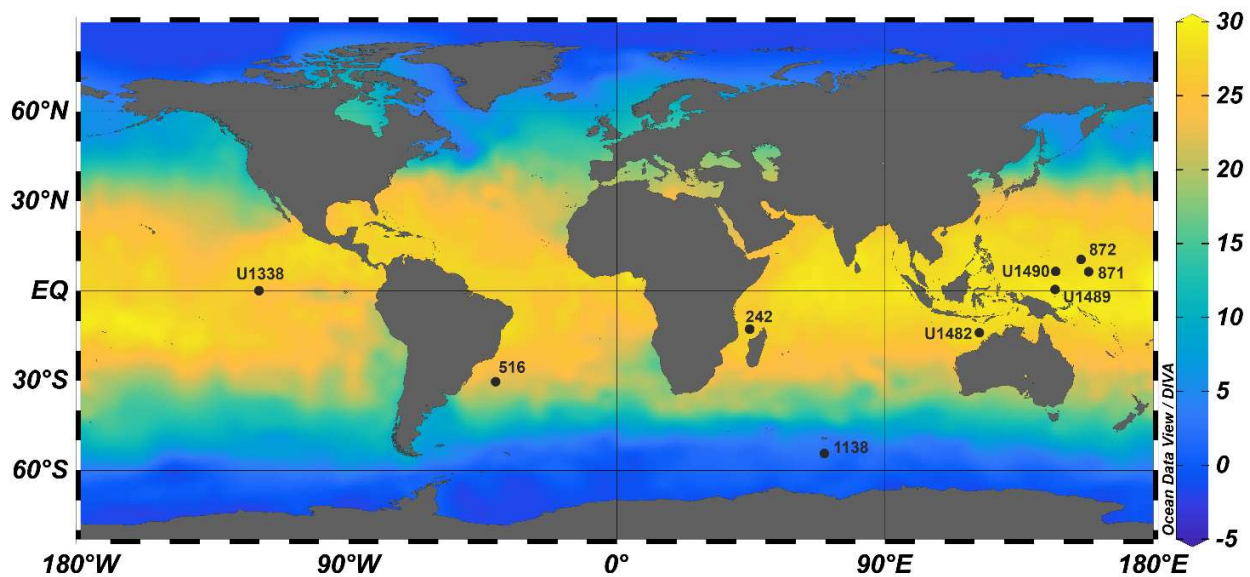
98 **2.1 Material**

99 The dataset (Boscolo-Galazzo, Crichton et al., 2021) was produced from a range of globally and
100 latitudinally distributed DSDP (Deep Sea Drilling Program), ODP (Ocean Drilling Program), and
101 IODP (Integrated Ocean Drilling Program/International Ocean Discovery Program) sites (Fig. 1)
102 which are high in carbonate and composed of calcareous nannofossils and foraminiferal pelagic
103 oozes, with some input of siliceous plankton. Sites were selected based on the best available global
104 and temporal coverage and preservation of foraminifera. Planktonic foraminiferal preservation
105 ranges from excellent to very good (recrystallized but lacking overgrowth and infilling) (Boscolo-
106 Galazzo, Crichton et al., 2021) with the exception of Sites U1490 and U1489, where there is some
107 overgrowth and infilling in the middle Miocene (Fayolle and Wade, 2020; Boscolo-Galazzo,
108 Crichton et al., 2021). The target time intervals selected for sampling were 0, 2.5, 4.5, 7.5, 10, 12.5
109 and 15 Ma. Biostratigraphic analysis was used to assess age using the biochronology of Wade et
110 al. (2011) calibrated to the time scale of Lourens et al. (2004) (Supplementary Table 1).

111 **2.2 Planktonic foraminifera**

112 Fifty-nine species of planktonic foraminifera were analysed for Mg/Ca and $\delta^{18}\text{O}$. Planktonic
113 foraminiferal were picked from three constrained size fractions: 180-250 μm , 250-300 μm and
114 300-355 μm . Planktonic foraminiferal geochemistry can change through size (e.g., Birch et al.,
115 2013), so here we used data from the size fraction 250-355 μm only, giving a total of 57 species
116 in the dataset. For abundant species, up to 80 specimens were picked for geochemical analysis,

117 with as many as possible picked in the case of less common species. Hence, our foraminiferal data
118 represent an average from multiple specimens. Paleodepth habitat attributions follow Boscolo-
119 Galazzo, Crichton et al. (2021) and Boscolo-Galazzo et al. (2022). Planktonic foraminiferal
120 taxonomy follows the concepts described in Boscolo-Galazzo et al. (2022).



121

122 **Figure 1.** Site map with present-day mean annual sea surface temperatures (°C) from the World
123 Ocean Atlas 2013 (Locarnini et al., 2013).

124 2.3 Trace element and stable isotope analysis

125 Picked planktonic foraminifera were crushed between two glass slides to open all large chambers.
126 When there was enough material, the crushed sample was split for stable isotope and trace element
127 analysis. The trace element split was cleaned using a protocol to remove clays and organic matter
128 (step A1.1-A1.3 of Barker et al. (2003)). The samples did not undergo reductive cleaning due to
129 their fragility and small sample size, and because the reductive step may cause preferential removal
130 of high Mg/Ca calcite from the test (Yu et al., 2007). Samples were dissolved in trace metal pure
131 0.065 M HNO₃, then diluted with trace metal pure 0.5 M HNO₃ and analysed at Cardiff University

132 on a Thermo Fisher Scientific Element XR ICP-MS against standards with matched calcium
133 concentration to reduce matrix effects (Lear et al., 2002). Long term analytical precision
134 determined from consistency standards (CS1 and CS2) with Mg/Ca ratios of 1.24 mmol/mol and
135 7.15 mmol/mol are ~0.7 and ~0.8% (relative standard deviation). Mg/Ca was plotted against Fe/Ca
136 and Mn/Ca to assess whether there was any relationship as a result of the presence of Fe-Mn
137 oxyhydroxides affecting Mg/Ca, but there was no correlation between the contaminant indicators
138 and Mg/Ca (Supp. Fig. 1).

139 Stable isotopes were measured on a Delta V Advantage with Gasbench II mass spectrometer at the
140 Cardiff University stable isotope facility. Stable isotope results were calibrated to the VPDB scale
141 using an in-house carbonate standard (Carrara marble). Analytical precision was 0.05‰ for $\delta^{18}\text{O}$
142 and 0.05‰ for $\delta^{13}\text{C}$.

143 2.4 Data analysis

144 Before performing the analysis, we screened the dataset for outliers, and removed one anomalously
145 high datapoint with a Mg/Ca value >9 mmol/mol which we attributed to analytical error
146 (Supplementary Table 1).

147 2.4.1 Formulation of theoretical relationships between Mg/Ca and $\delta^{18}\text{O}$

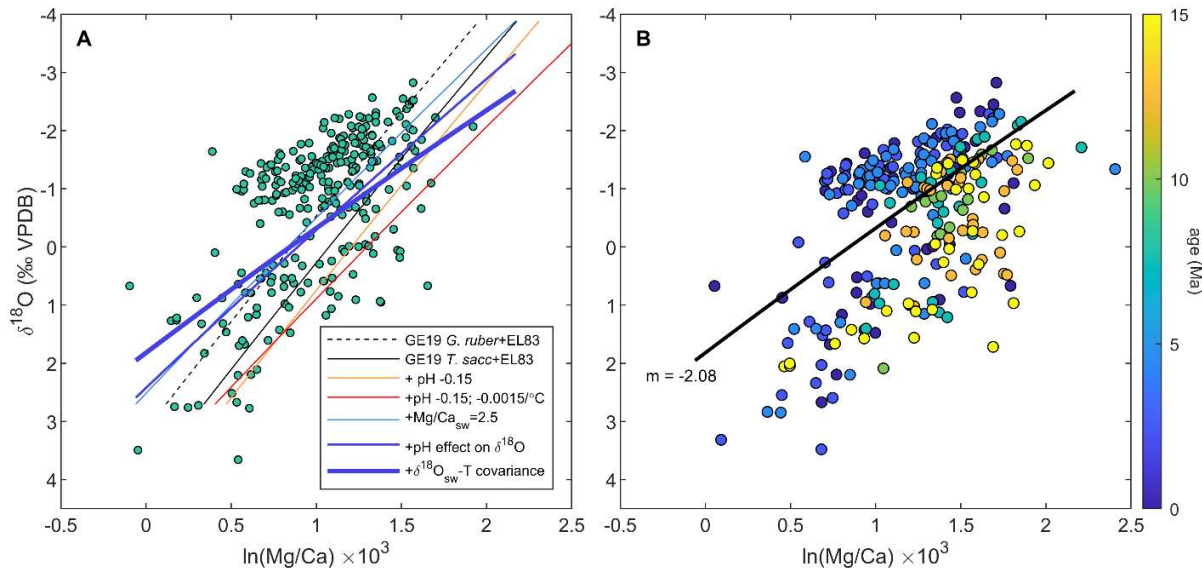
148 To test for covariation between Mg/Ca and oxygen isotope data, we regressed the data against each
149 other and compared the observed relationship with that expected from modern calibrations. We
150 did this to initially explore the dataset and what kind of relationship we might expect between
151 Mg/Ca and $\delta^{18}\text{O}$ and whether this manifests in the dataset, before applying corrections for the non-
152 thermal influences on both proxies. Given the complexity of the sample set (e.g., multiple species,
153 ages, locations, preservation), different expected relationships between Mg/Ca and $\delta^{18}\text{O}$ are

154 possible, which depend on: i) species-specific vital effects, ii) the non-thermal controls on Mg/Ca,
155 (salinity, pH, Mg/Ca_{sw}), iii) non-thermal controls on $\delta^{18}\text{O}$ (pH/[CO₃²⁻]), $\delta^{18}\text{O}_{\text{sw}}$, as well as how
156 these factors change through time. To account for this, we calculated a number of possible
157 expected theoretical relationships to give a sense of how much of the scatter in the raw data is
158 likely to be explicable by these factors and inform our following data-analysis accordingly. We
159 stress that this exercise was conducted as a mean of exploring the whole data set; no single
160 relationship will be able to explain the dataset because it is influenced by multiple, often
161 interlinked, variables.

162 Expected theoretical relationships were calculated starting with modern laboratory culture
163 calibrations, onto which the key non-thermal long-term and spatial controls on these proxies were
164 sequentially added to demonstrate how much each of these is expected to shift the slope of the
165 expected Mg/Ca- $\delta^{18}\text{O}$ relationship (Fig. 2A). Specifically, we i) combined the Mg/Ca temperature
166 calibrations for *Globigerinoides ruber* and *Trilobatus sacculifer* of Gray & Evans (2019) with the
167 $\delta^{18}\text{O}$ -temperature equation of Erez & Luz (1983), ii) added the impact of a 0.15 unit whole ocean
168 pH change (approximating the magnitude of the Neogene whole ocean change, e.g., Rae et al.,
169 2021) using the pH-Mg/Ca slope for *G. ruber* as an example (note that this is only applicable to
170 species that show a pH sensitivity) (Evans et al., 2016a), iii) included the expected control of
171 temperature on pH via the T-dependent dissociation of water (K_w), i.e., temperature-driven pH
172 changes within a given time interval independent of whole ocean pH shifts (Gray et al., 2018), iv)
173 showed the impact of Mg/Ca_{sw} half of the modern ratio (Evans et al., 2016b), v) included the effect
174 of pH or [CO₃²⁻] on $\delta^{18}\text{O}$ (Spero et al., 1997; Zeebe, 1999) given the covariance of temperature
175 and pH described in point iii above using the multispecies average slope of Gaskell et al. (2023),
176 and finally vi) explored the likely impact of the covariance of $\delta^{18}\text{O}_{\text{sw}}$ and temperature that is

177 characteristic of the modern ocean and arises from the broad coupling of the hydrological cycle
178 with surface temperatures. Specifically, this latter influence was calculated by combining SST data
179 from the 2013 World Ocean Atlas (Locarnini et al., 2013) and $\delta^{18}\text{O}_{\text{sw}}$ from LeGrande & Schmidt
180 (2006), taking all surface ocean data except that from polar meltwater regions, which demonstrates
181 that, on average, in the modern ocean $\delta^{18}\text{O}_{\text{sw}}$ increases by 0.0425 ‰ per °C SST increase.
182 Each of these factors was applied additively such that (e.g.) the fourth factor listed above
183 ($\text{Mg}/\text{Ca}_{\text{sw}}$) in Fig. 2 includes numbers 1 through 3. The sum of the influence of these factors on
184 the theoretical $\delta^{18}\text{O}$ -Mg/Ca relationship is represented by the thick blue line in Figure 2A and the
185 black line in Figures 3, 6, 7 and 8, which has a slope of -2.08 in $\delta^{18}\text{O}$ - $\ln(\text{Mg}/\text{Ca})$ space.
186 The magnitude of some of these potential non-thermal controls on the two proxies over the time
187 interval studied here are reasonably well constrained. Specifically, the long-term whole ocean pH
188 and $\text{Mg}/\text{Ca}_{\text{sw}}$ changes are sufficiently well known (Rae et al., 2021; Zhou et al., 2021; Brennan et
189 al., 2013) that they can be “subtracted” out of the raw proxy values, given that they are likely to
190 apply to all or most species in the dataset. As such, we next explored the degree to which the
191 Mg/Ca - $\delta^{18}\text{O}$ covariation improves once long-term whole ocean pH and $\text{Mg}/\text{Ca}_{\text{sw}}$ changes are
192 removed. To avoid (possibly incorrect) a-priori assumptions regarding, for example, which
193 Mg/Ca -temperature calibration should be applied to each species in the dataset and the degree to
194 which surface ocean $\delta^{18}\text{O}_{\text{sw}}$ has varied at the study sites, we initially did this keeping the Mg/Ca
195 and $\delta^{18}\text{O}$ comparison in raw proxy space and: 1) converted the raw Mg/Ca values to temperature
196 using the multispecies Mg/Ca -temperature calibration from Gray and Evans (2019), together with
197 our best estimate of pH and $\text{Mg}/\text{Ca}_{\text{sw}}$ (as described below (§2.4.2)), and 2) converted the
198 temperatures back into Mg/Ca using the same calibration but modern seawater Mg/Ca and pH.
199 Conceptually, this is equivalent to correcting the raw proxy values for these nonthermal controls.

200 In addition, we subtracted out the long-term whole ocean change in $\delta^{18}\text{O}_{\text{sw}}$ related to continental
 201 ice growth using the sea level curve of Rohling et al. (2022) and a sea level- $\delta^{18}\text{O}_{\text{sw}}$ scaling factor
 202 of 1‰ per 67 m. This results in a raw proxy dataset in which the aforementioned long-term non-



203
 204 **Fig. 2.** Raw $\delta^{18}\text{O}$ plotted against Mg/Ca for all samples presented here. (A) Several possible expected
 205 Mg/Ca- $\delta^{18}\text{O}$ slopes are shown for comparison, including that for *G. ruber* and *T. sacculifer* (at constant pH)
 206 in the modern ocean (solid and dashed black lines respectively). The additive impact of nonthermal controls
 207 are then explored using the *G. ruber* calibration as an example, specifically, the impact of: a whole-ocean
 208 pH shift of 0.15 units (orange line), accounting for the covariation of pH and temperature (driven by the
 209 temperature-dependent dissociation of water, red line), seawater Mg/Ca half of the present day value (thin
 210 blue line), the theoretical impact of pH on $\delta^{18}\text{O}$ (blue line), and the covariance of temperature and $\delta^{18}\text{O}_{\text{sw}}$ in
 211 the modern ocean (thick blue line). We stress that the magnitude of the pH, Mg/Ca_{sw}, and $\delta^{18}\text{O}_{\text{sw}}$ changes
 212 applied to these theoretical lines were chosen to illustrate the sensitivity of the two proxies to these factors
 213 and do not necessarily represent the degree to which these factors differed in any specific time interval
 214 compared to today. The length of each line depicts the expected Mg/Ca and $\delta^{18}\text{O}$ change across the same
 215 temperature range in each case (5–35°C). All calculations assume $\delta^{18}\text{O}_{\text{sw}} = 0\text{‰}$. (B) As in panel A, except
 216 with the long-term whole ocean changes in pH, Mg/Ca_{sw}, and $\delta^{18}\text{O}_{\text{sw}}$ subtracted from the raw proxy values
 217 (see text, using the multispecies calibration of Gray & Evans (2019) in the case of the Mg/Ca corrections),
 218 i.e., accounting for the impact of these non-thermal Mg/Ca and $\delta^{18}\text{O}$ controls. Sample age is shown as a
 219 function of colour. Note that the black line is not a regression but rather shows one possible theoretical
 220 Mg/Ca- $\delta^{18}\text{O}$ relationship and is identical to the thick blue line from panel A including the combined effect
 221 of all factors explored there. The slope of this theoretical relationship is -2.08, which provides an
 222 approximate expected slope of Miocene-Recent Mg/Ca versus $\delta^{18}\text{O}$, although we note that no real-world
 223 dataset will conform exactly to this as pH, Mg/Ca_{sw}, and $\delta^{18}\text{O}_{\text{sw}}$ have not (perfectly) covaried through time.

224

225 thermal factors are no longer present and which can be used to evaluate the occurrence of residual
226 scatter independent of the long term non-thermal controls on Mg/Ca and $\delta^{18}\text{O}$ (Fig. 2B).

227 2.4.2 Transformation of proxy values into paleotemperature

228 Measured foraminifera Mg/Ca was transformed into paleotemperature using the *MgCaRB* tool
229 (Gray & Evans, 2019; <https://github.com/willyrgray/MgCaRB> (R);
230 <https://github.com/dbjevans/MgCaRB> (Matlab)) which takes into account:

- 231 - Salinity. Although this has a minor effect on Mg/Ca (Hönisch et al., 2013), whole ocean
232 changes are nonetheless accounted for using a salinity reconstruction derived from scaling
233 the $\delta^{18}\text{O}$ benthic stack (Westerhold et al., 2020) to the sea level record of Spratt & Lisiecki
234 (2016), which is then applied to derive sea level between 0.8 and 8 Ma, before which that
235 of Rohling et al. (2022) was used, rescaled to match the $\delta^{18}\text{O}$ -derived reconstruction at 8
236 Ma and a sea level of +67 m in an ice-free world at 50 Ma. We applied the multispecies
237 salinity sensitivity of Gray & Evans (2019) to all species (3.6% per salinity unit).
- 238 - pH. Long-term whole ocean changes were derived from a smoothing spline fit to the boron
239 isotope-derived pH data compiled by Rae et al. (2021). We applied species-specific pH-
240 Mg/Ca sensitivities of Gray & Evans (2019) where available for a given species/lineage
241 (discussed in more detail below) and used the multispecies sensitivity in all other cases.
- 242 - Mg/Ca_{sw} was derived by combining the [Ca²⁺_{sw}] record of Zhou et al. (2021) with a
243 smoothing spline fit to the fluid inclusion [Mg²⁺_{sw}] data given in Brennan et al. (2013).
244 Raw Mg/Ca values were adjusted using the equation Mg/Ca_{corrected} = Mg/Ca_{raw} ×
245 Mg/Ca_{sw}^H/5.2^H, where H = 0.64 based on a data compilation of three foraminifera species
246 and inorganic calcite (Holland et al., 2020; Evans et al., 2015; 2016b; Mucci & Morse,
247 1983).

248 We initially applied a multispecies equation, because the dataset includes a mix of extant and
249 extinct species, some of these never measured for trace elements before (Supplementary Table 2),
250 or lacking an extant/well-calibrated modern relative. Specifically, we used the multispecies
251 Mg/Ca-temperature equation of Gray & Evans (2019) and applied the multispecies pH, salinity,
252 and temperature sensitivities, together with the *Globigerinoides ruber* pre-exponential coefficient
253 (given a Mg/Ca-T relationship of the form $Mg/Ca = BeAT$ in its simplest form) as most of the
254 species for which high quality data exist are known to be characterized by a Mg/Ca-pH sensitivity
255 (Lea et al., 1999; Kisakürek et al., 2008; Evans et al., 2016a).

256 We subsequently applied species-specific calibrations to selected lineages to explore the degree to
257 which scatter in the dataset can be accounted for by taking into account phylogenetic relationships
258 among ancestor-descendent species. Specifically, the *Trilobatus sacculifer* calibration was applied
259 to the *Trilobatus trilobus* - *Trilobatus sacculifer* lineage, and the *Orbulina universa* calibration
260 was applied to the *Preorbolina-Orbulina* lineage, both from laboratory culture studies following
261 Gray & Evans (2019). To *Neogloboquadrina* and its descendent lineage *Pulleniatina* we applied
262 a *Neogloboquadrina pachyderma* calibration with the sensitivities (and their uncertainties) of
263 Tierney et al. (2019) (implemented with a re-fit to the dataset following the *MgCaRB* approach,
264 see Figure S1). We then evaluate the improvement relative to the multispecies calibration in
265 samples spanning the middle Miocene to modern. The attribution of phylogenetic relationships
266 follows Aze et al. (2011), Spezzaferri et al. (2018), Leckie et al. (2018) and Fabbrini et al. (2021).
267 All uncertainties were fully propagated via Monte Carlo simulation, including those related to:
268 analysis, calibration coefficients (the coefficients that relate Mg/Ca to temperature, pH, and
269 salinity), and the 95% confidence intervals on the salinity, pH, and Mg/Ca_{sw} reconstructions.
270 Specifically, 10^4 random draws of each of these values within their respective uncertainty bounds

271 were used to generate the reported values and 95% CI (2.5th, 50th, and 97.5th percentiles of the
272 resulting dataset). The relative contributions of the various nonthermal factors impacting Mg/Ca-
273 derived temperature are shown in Figure S2.

274 The conversion of $\delta^{18}\text{O}$ to paleotemperature followed Gaskell et al. (2023) using: the bayfox
275 calibration (Malevich et al., 2019) and the global and local $\delta^{18}\text{O}_{\text{sw}}$ of Rohling et al. (2022) and
276 Gaskell et al. (2023) respectively. The calculation was performed twice, both with and without a
277 pH/[CO₃²⁻] effect on $\delta^{18}\text{O}$ (the former using the mean planktonic foraminiferal slope of Gaskell et
278 al. (2023) and the [CO₃²⁻] record of Zeebe & Tyrrell (2019)). We also explored the impact of using
279 a different sea level/deep ocean temperature reconstruction (Miller et al., 2020) on our results,
280 described in the Results Section and shown in Figure S3.

281 When evaluating the paleotemperature reconstructions, we define whether or not the two proxy
282 systems agree within uncertainty by determining if the root sum of squares of the two uncertainties
283 is smaller than the temperature difference between the two proxies. We then proceed to identify
284 possible drivers for the data deviating from the expected Mg/Ca and $\delta^{18}\text{O}$ relationship by
285 evaluating the age of the sample, regional changes in $\delta^{18}\text{O}$ seawater, depth ecology, and possible
286 species-specific offsets.

287 We note that all of the above corrections assume surface ocean conditions, while the dataset
288 contains a number of species that calcify at depth (Boscolo-Galazzo et al., 2021). Given the
289 uncertainties surrounding past changes in vertical pH and $\delta^{18}\text{O}_{\text{sw}}$ profiles, we do not attempt to
290 account for this in our data analysis but note that this consideration should be borne in mind when
291 interpreting data from deep-dwelling species.

292 **3. Results**

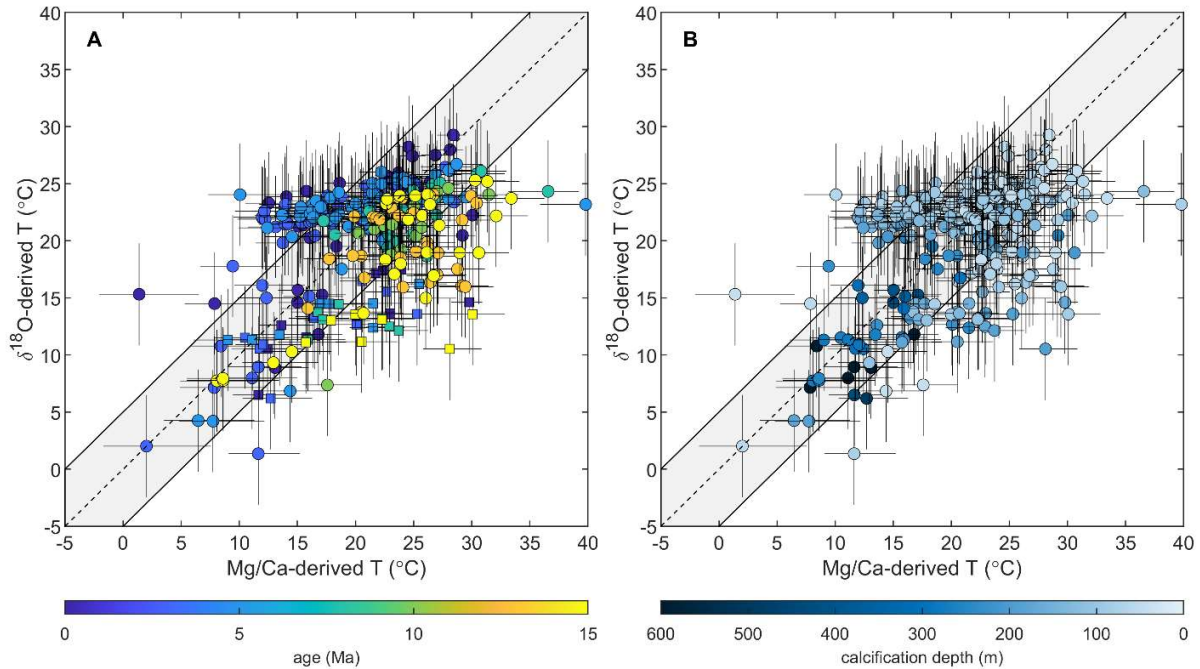
293 Our basic expectation is that higher Mg/Ca should relate to more negative $\delta^{18}\text{O}$ values for warmer
294 temperatures, and *vice versa* for colder temperatures. Despite the large number of variables
295 included, the dataset as a whole shows a significant correlation (Fig. 2A; $R^2 = 0.37$, RMSE = 1.01,
296 $p << 0.01$) between $\delta^{18}\text{O}$ and $\ln(\text{Mg/Ca})$. Hence, the $\delta^{18}\text{O}$ -Mg/Ca covariance can be considered a
297 robust feature over the past 15 Myr for the majority of the species analyzed and across the study
298 sites. Nonetheless, there is a high degree of scatter in the data which suggests that the temperature
299 signal which should lead Mg/Ca and $\delta^{18}\text{O}$ data to change consistently in opposite directions is
300 affected by other factors. Our exercise of generating theoretical Mg/Ca- $\delta^{18}\text{O}$ relationships (Fig.
301 2A), exploring how the relationship between the two proxies might change through space and time,
302 provides a qualitative indication as to whether the scatter can be attributed to long term non-
303 thermal factors generally corrected for when using the $\delta^{18}\text{O}$ and Mg/Ca proxies. The substantial
304 differences between these expected relationships suggests that this is likely to be the case (Fig.
305 2A). In particular, Fig. 2A suggests that both a pH effect and Mg/Ca_{sw} changes through time may
306 explain a substantial degree of the variability observed in the dataset compared to the modern
307 relationships (compare the coloured and black lines, see also Figure S2). Nonetheless, accounting
308 for these long-term biases alone in the raw dataset does not remove the scatter (Fig. 2B), suggesting
309 the importance of additional factors, such as vital effects and regional variations in $\delta^{18}\text{O}_{\text{sw}}$. Data
310 converted into temperature, along with 95% confidence intervals, are shown in Figure 3. In this
311 plot 62% of the data points fall within uncertainty, confirming that a high degree of variability in
312 the raw data can be effectively explained and accounted for by correcting for the known spatially
313 and temporally varying non-thermal effects influencing both proxies.

314 Using the deep ocean temperature and sea level records of Miller et al. (2020) rather than Rohling
315 et al. (2022) (Figure S3) would shift our $\delta^{18}\text{O}$ temperature reconstructions of +0.5-3.3°C

316 depending on sample age, with the samples from the 7.5 Ma time slice being mostly affected.
317 Whilst the choice of the record to correct for global $\delta^{18}\text{O}_{\text{sw}}$ exerts a significant control on $\delta^{18}\text{O}$ -
318 derived temperatures, it has a minor impact both on our long-term dataset overall (compare Fig. 3
319 with Figure S3) and the proportion of proxy data within combined uncertainty, from 62% to 64%.
320 We find that deep-dwelling and surface-dwelling species fall within uncertainty in terms of the
321 broad degree of agreement between Mg/Ca and $\delta^{18}\text{O}$ derived temperatures, hence different depth-
322 habitat ecologies or calcification environments do not represent a systematic source of offset *per*
323 *se* (Fig. 3B). Indeed, all the species displaying a temperature offset between the two proxies are
324 surface-dwellers (0-200 m depth, Boscolo-Galazzo et al., 2022), with deep-dwellers characterized
325 by inter-proxy agreement in almost all cases (Fig. 3B). Additional explanations are required for
326 those temperature reconstructions that, all non-thermal and spatial controls included, still plot
327 outside their propagated error uncertainty. The data points outside the combined proxy
328 uncertainties either display $>5^\circ\text{C}$ warmer (colder) $\delta^{18}\text{O}$ (Mg/Ca) temperatures (upper left area of
329 the plot) or $>5^\circ\text{C}$ warmer (colder) Mg/Ca ($\delta^{18}\text{O}$) temperatures (bottom right area of the plot) (Fig.
330 3).

331

332



333

334 **Fig. 3.** $\delta^{18}\text{O}$ versus Mg/Ca-derived paleotemperatures plotted as function of age (A) and calcification depth
 335 (B), accounting for the impact of whole ocean and regional changes in $\delta^{18}\text{O}_{\text{sw}}$ following Gaskell *et al.* (2022)
 336 and the bayfox $\delta^{18}\text{O}$ -temperature calibration (Malevich *et al.*, 2019), whole ocean changes in Mg/Ca_{sw} and
 337 pH on Mg/Ca using MgCaRB (Gray & Evans, 2019), and including a pH correction on $\delta^{18}\text{O}$ using the mean
 338 planktonic foraminifera slope (Gaskell *et al.*, 2023). Fully propagated uncertainties in both proxies are
 339 shown, incorporating analysis, calibration, pH, Mg/Ca_{sw}, $\delta^{18}\text{O}_{\text{sw}}$ /salinity (see text for details). Site 516 data
 340 are shown with square symbols in panel A.

341

342 Figure 3A clearly shows that the large majority of the outliers in the upper left part of the plot
 343 (warmer $\delta^{18}\text{O}$ temperatures or cooler Mg/Ca temperatures) are species of late Miocene to modern
 344 age, while the outliers in the bottom right part of the plot (warmer Mg/Ca temperatures) are mostly
 345 older species of middle Miocene age or from mid-latitude Site 516 (squares in Fig. 3C). We suggest
 346 and discuss possible main sources for these offsets between Mg/Ca and $\delta^{18}\text{O}$ temperatures in detail
 347 below.

348 **4. Discussion**

349 **4.1 Diagenesis**

350 Diagenesis is known to alter the test chemistry of foraminifera in three main ways: partial
351 dissolution, overgrowth, and recrystallization (Edgar et al., 2015). The trace element and isotopic
352 composition of tests react differently to these diagenetic processes. The trace element composition
353 of foraminiferal calcite may be susceptible to partial dissolution because it is inhomogeneous
354 (Fehrenbacher et al., 2014), which decreases trace element ratios in species with high and low-Mg
355 regions (Dekens et al., 2002; Edgar et al., 2015; Rongstad et al., 2017), resulting in lower
356 temperature reconstructions. Overgrowth and recrystallization have been shown to add both low-
357 Mg and high-Mg diagenetic calcite, potentially impacting the original signal in opposite directions
358 (Branson et al., 2015), although Mg/Ca is relatively robust to this type of diagenesis, at least in
359 certain circumstances (Staudigel et al., 2022). The oxygen isotopic composition of planktonic
360 foraminiferal tests is well known to be very sensitive to overgrowth and recrystallization (e.g.
361 Sexton et al., 2006), whereby the addition of diagenetic calcite, or the replacement of the original
362 calcite with diagenetic calcite precipitated at the seafloor, can significantly alter the original
363 isotopic signal shifting it to more positive values (Pearson, 2012; Edgar et al., 2015).

364 The Boscolo-Galazzo, Crichton et al. (2021) dataset spans 15 million years and includes sites with
365 different average preservation of foraminiferal tests and oceanographic settings. When the data are
366 regressed against each other (Fig. 2B), we find a total of 26 data points characterized by oxygen
367 isotope values more positive than expected from their Mg/Ca values (Fig. 2B; Supplementary
368 Table 1), resulting in $\delta^{18}\text{O}$ temperatures $>5^\circ\text{C}$ colder than Mg/Ca temperatures (outside the error
369 envelope) (Fig. 3; Supplementary Table 1). Twenty-one of these data points were from the older
370 time slices (12.5 and 15 Ma), one from the 7.5 Ma time slice and four from the core-top of Site
371 U1338 (Supplementary Table 1).

372 As the majority of these data points were characterized by Mg/Ca values of \sim 1.5-2 $\ln(\text{Mg/Ca})$ (Fig.
373 2B), this yielding more reasonable Mg/Ca than $\delta^{18}\text{O}$ temperatures for these sites/time intervals
374 (Supplementary Table 1), the observed offset is most likely best attributed to diagenetic
375 overgrowth/recrystallization, shifting oxygen isotopes towards more positive values without
376 affecting Mg/Ca to the same extent. A recent study compared typical Mg/Ca- $\delta^{18}\text{O}$ from
377 recrystallized planktonic foraminifera with chemical diffusive models simulating early diagenetic
378 processes in calcite (Staudigel et al., 2022). According to that study, in a closed system, the bulk
379 $\delta^{18}\text{O}$ value will be altered faster than the Mg/Ca, regardless of what partitioning coefficient is used
380 for Mg, leading to a progressive shift to more positive $\delta^{18}\text{O}$ values leaving Mg/Ca virtually
381 unchanged (Staudigel et al., 2022).

382 The datapoints presenting $\delta^{18}\text{O}$ overprinted by overgrowth/recrystallization were distributed
383 across most of the study sites (except for Sites 871/872), but they were more common at Site
384 U1490 and U1489 (15/26) which are characterized by inferior preservation compared to the others
385 (Boscolo-Galazzo, Crichton et al., 2021). The core-top samples at Site U1338 show clear signs of
386 dissolution with highly fragmented tests. These data points presented the lowest Mg/Ca values in
387 the dataset (1.68 and 0.91 mmol/mol) with temperatures from Mg/Ca lower than from $\delta^{18}\text{O}$. This
388 suggests that partial dissolution and recrystallization affected both Mg/Ca and $\delta^{18}\text{O}$ in this sample,
389 but Mg/Ca more so.

390 Overall, our scrutiny for diagenesis of the Boscolo-Galazzo, Crichton et al., (2021) dataset is
391 consistent with previous studies suggesting that $\delta^{18}\text{O}$ values are more easily affected by
392 recrystallization than Mg/Ca (Sexton et al., 2006; Staudigel et al., 2022; John et al., 2023), similar
393 to other trace element systems (Edgar et al., 2015).

394 Based on the considerations above we excluded the affected 26 data points from the subsequent
395 analysis as being characterized by a stronger diagenetic overprint than the rest of the dataset
396 (Supplementary Table 1). Removing the affected data points in some but not all the cases equated
397 to removing a whole sample (Supplementary Table 1). This is because of variable diagenetically
398 offset $\delta^{18}\text{O}$ values from different species in a sample, as observed elsewhere (Sexton et al., 2006;
399 Edgar et al., 2015). The approach used here to reconstruct $\delta^{18}\text{O}$ temperature shows that for the
400 majority of the study dataset a diagenetic offset would be comprised within the propagated error
401 envelope ($\sim 2\text{--}2.5^\circ\text{C}$) (Fig. 3) and comparable or not distinguishable from an offset deriving from
402 poorly constrained $\delta^{18}\text{O}_{\text{sw}}$.

403 4.2 Regional scale spatial heterogeneity in seawater chemistry

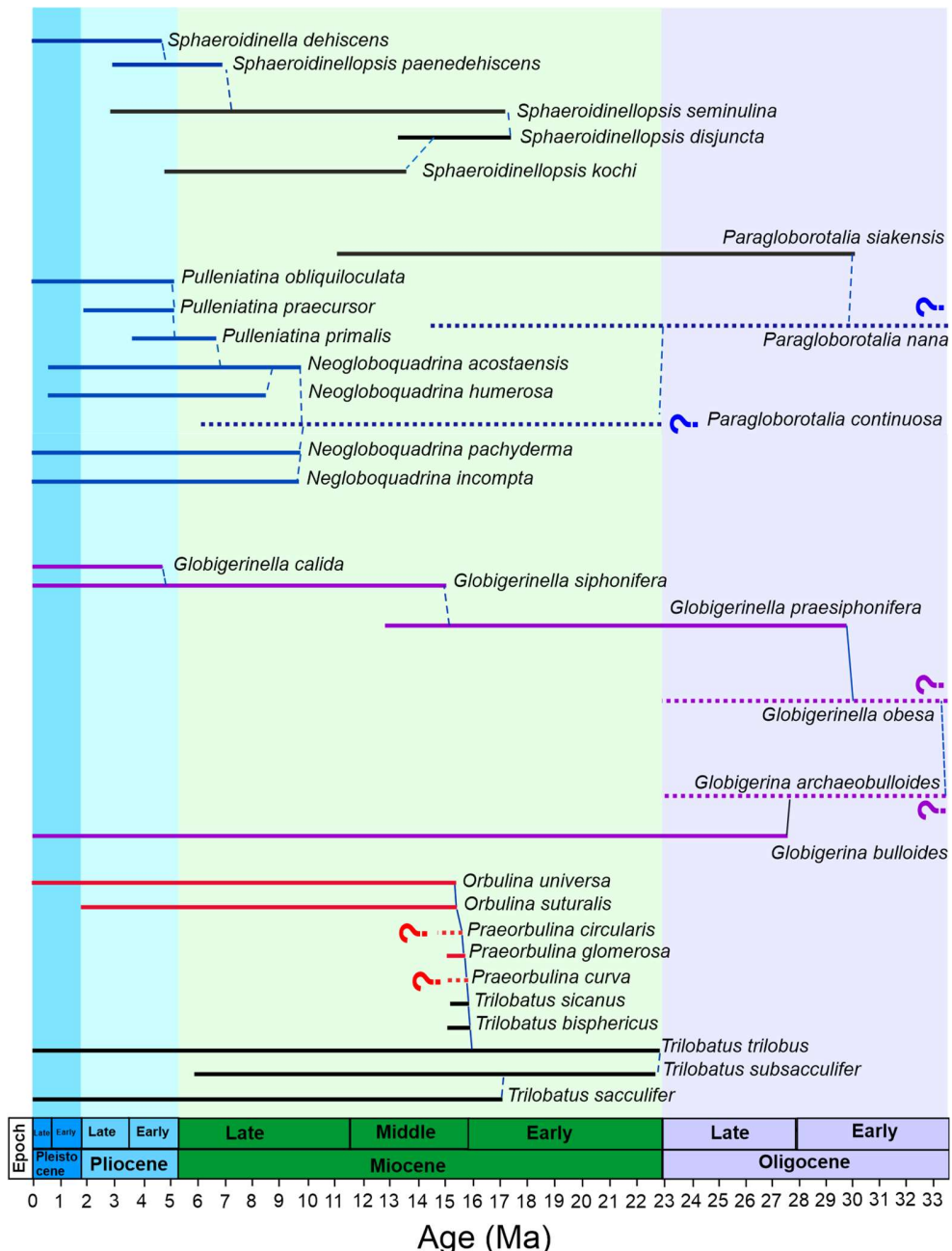
404 Once converted into temperatures the dataset shows an overall good agreement of Mg/Ca- $\delta^{18}\text{O}$
405 data, consistent with temperature being a dominant controller of both proxies through time and
406 across the broad geographical area investigated (Fig. 3). This suggests that, by and large, the
407 seawater corrections applied for the local and global changes in ocean chemistry are adequate,
408 although for one site this may not hold true. Site 516 is a mid-latitude site (south-west Atlantic,
409 30°S) characterized by a modern sea surface temperature around 20°C (Fig. 1), most of the data
410 points from this site have very positive $\delta^{18}\text{O}$ values associated with high Mg/Ca (Fig. 2B;
411 Supplementary Table 1). Once converted, this results in $\delta^{18}\text{O}$ temperatures that are too cold (12--
412 17°C) compared to both modern (given long-term warming since the Miocene is not expected at
413 any of these sites) and the equivalent Mg/Ca temperatures from the same samples, which are
414 around $21\text{--}25^\circ\text{C}$ (Fig. 3A; Supplementary Table 1). We do not attribute this mismatch to diagenesis
415 for a number of reasons. First, Site 516 is characterized by a very good test preservation, much
416 better than at Site U1489 and U1490 for which diagenesis extensively affects the middle Miocene

417 samples; second, this mismatch is observed in the entire dataset through samples spanning the
418 middle Miocene to modern; third, the mismatch is observed for surface-dwelling species only,
419 with deep-dwellers characterised by $\delta^{18}\text{O}$ - Mg/Ca in good agreement. Because of its location, Site
420 516 is situated in an area of complex surface hydrography, as it sits at the confluence between the
421 warm Brazil Western Boundary Current and the cold Falkland (Malvinas) Current spinning off
422 from the Antarctic Circumpolar Current (e.g., Jonkers et al., 2021). Compared to the subtropical
423 gyres, where many of the study samples come from, a large degree of spatial variability of surface
424 water physical-chemical properties can be expected on a seasonal and multiannual scale. As such,
425 we suggest that the mismatch between $\delta^{18}\text{O}$ and Mg/Ca observed in surface dwelling species at
426 Site 516 may result from changeable surface water properties from the mixing of two very different
427 water masses creating deviations in pH, salinity and $\delta^{18}\text{O}_{\text{sw}}$ beyond those that are typical in
428 stratified open ocean environments and that are difficult to correct for. Sites with a changeable
429 hydrography such Site 516, may hence not be ideal for the application of geochemical proxies
430 affected by seawater chemistry, unless changes in seawater chemistry at the site can be
431 reconstructed directly.

432 4.3 Species-specific offsets

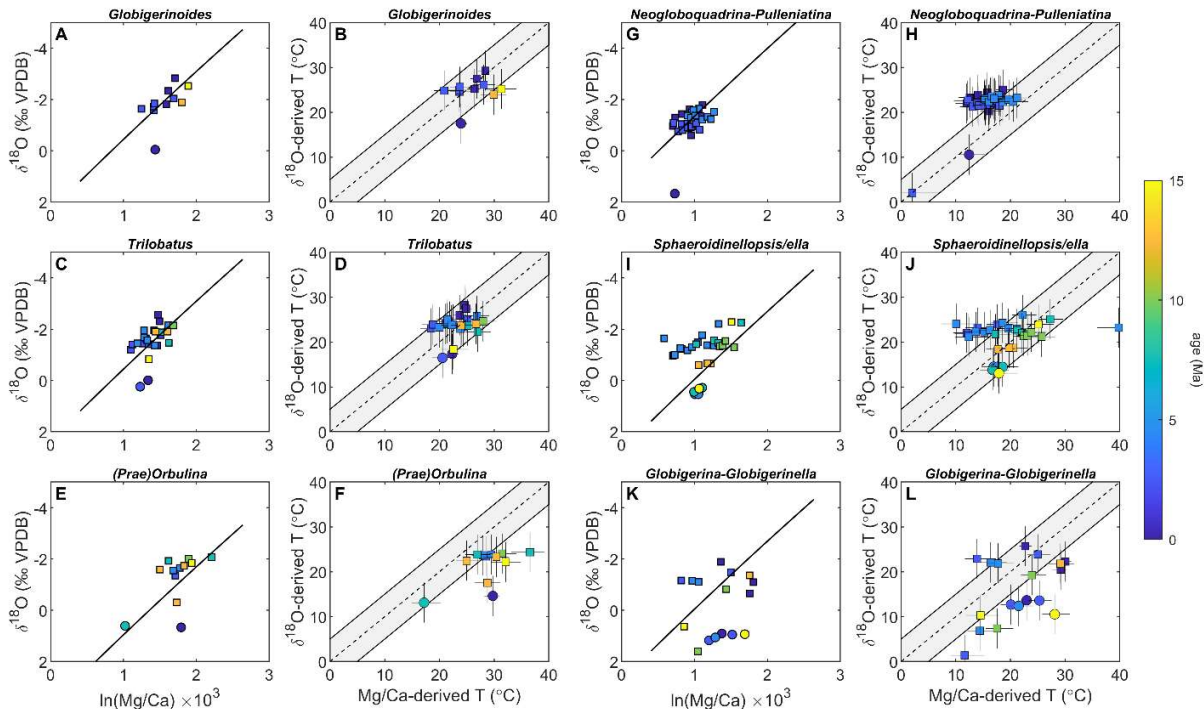
433 The third and largest source of mismatch that we consider is the occurrence of species-specific
434 offsets, particularly in Mg/Ca given that, in general, the relative degree of inter-species Mg/Ca
435 variability is greater than for shell oxygen isotope composition. For example, the range of inter-
436 species $\delta^{18}\text{O}$ offsets is around 1‰ (<4°C), whereas there may be more than a factor of two
437 difference in Mg/Ca between species for a given temperature (e.g., compare Pearson, 2012; Gray
438 & Evans, 2019, Regenberg et al., 2009; Däeron & Gray, 2023). When regressing the data against
439 each other, we find several species presenting systematically offset Mg/Ca values (e.g., Fig. 2B;

440 Supplementary Table 1) leading to proxy-proxy disagreement (Fig. 3; Supplementary Table 1).
441 The occurrence of such offset Mg/Ca values is not evenly distributed across species, but is shared
442 among related species in both spinose and non-spinose groups (Figs. 4-5; Supplementary Table 1).
443 Specifically, the spinose species *Orbulina universa* (2 out of 5 specimens, 2/5), *O. suturalis* (3/6)
444 and *Praeorbulina glomerosa* (1/1) present high Mg/Ca ratios compared to their $\delta^{18}\text{O}$ values and
445 Mg/Ca of other species (Fig. 5E). We also find that *Globigerinella siphonifera* (6/7), *G. calida*
446 (1/1), *G. praesiphonifera* (3/4) and *Globigerina bulloides* (5/6) have offset Mg/Ca- $\delta^{18}\text{O}$ values,
447 largely being characterized by higher-than-expected Mg/Ca, although three *G. siphonifera* data
448 points show lower Mg/Ca (Figs. 4, 5K; Supplementary Table 1). Among non-spinose species:
449 *Neogloboquadrina humerosa* (11 out of 12 specimens, 11/12), *N. acostaensis* (3/3), *Pulleniatina*
450 *obliquiloculata* (5/6), *P. precursor* (3/5), *P. primalis* (4/6), *Sphaeroidinella dehiscens* (4/4), and
451 *Sphaerodinellopsis paenedehiscens* (5/10), display Mg/Ca values lower than expected for their
452 oxygen isotope composition (Figs. 4, 5 G, I; Supplementary Table 1).
453 These results highlight for the first time the occurrence of similarly offset Mg/Ca values for
454 ancestor-descent species belonging to the same lineage as well as for whole new lineages (Figs.
455 4,5).



456

457 **Fig. 4.** Phylogenetic relationships of offset spinose and non-spinose species. Shown here are the species
458 discussed in the text, their most closely related species and ancestors. Colored lines indicate species offset
459 in Mg/Ca in the study dataset relative to a multispecies calibration approach, black lines indicate non-offset
460 species. Red lines indicate offset species with higher Mg/Ca, blue lines offset species with lower Mg/Ca,
461 and purple lines species displaying both types of offsets. Question marks indicate the lack of Mg/Ca data
462 for a given species in the dataset presented here. Phylogeny after Aze et al. (2011) and Spezzaferri et al.
463 (2018). The phylogenetic chart was generated using Mikrotax (Huber et al., 2016;
464 www.mikrotax.org/pforams). Ages are from Lourens et al. (2004) for the Neogene and Pälike et al. (2006)
465 for the Oligocene.



466

467 **Fig. 5** $\delta^{18}\text{O}$ versus Mg/Ca and proxy-derived paleotemperature estimates for the ancestor-
468 descendant species *Globigerinoides subquadratus* – *G. ruber* (panels A and B), *Trilobatus trilobus*
469 – *T. sacculifer* (panels C and D), *Praeorbulina glomerosa* – *Orbulina suturalis* – *O. universa*
470 (panels E and F), *Neogloboquadrina acostaensis* – *N. humerosa*, *N. pachyderma* – *N. incompta*,
471 *N. acostaensis* – *Pulleniatina primalis* – *P. praecursor* – *P. finalis* (panels G and H),
472 *Sphaerodinellopsis seminulina* – *S. paenedehiscens* – *Sphaerodinella dehiscens*, *S. seminulina* –
473 *S. kochi* (panels I and J), *Globigerinella praeshiponifera* – *G. siphonifera* – *G. calida* and
474 *Globigerina bulloides* (panels K and L). Species are defined as offset relative to a multispecies
475 calibration approach when their reconstructed temperature plots outside the gray error envelope
476 (see text for details). Circles indicate data points from Site 516. Raw proxy values are given with
477 the long-term non-thermal controls on Mg/Ca subtracted out (as in Fig. 2), as well as an estimate
478 of paleotemperature (as in Fig. 3). The black lines depict one possible estimate of the expected
479 slope between $\delta^{18}\text{O}$ and Mg/Ca (the blue line from Fig. 2), adjusted to approximately match the
480 location of the data by shifting them in the direction of $\delta^{18}\text{O}$. Datapoints which are considered
481 strongly affected by diagenesis are not included in this plot. Note that one datapoint in panel G
482 falls outside of the plot area.

483

484 Divergent Mg/Ca values for *G. siphonifera* and *O. universa* have previously been reported
485 (Opdyke and Pearson, 1995; Anand et al., 2003; Friedrich et al., 2012). In the case of *O. universa*,
486 the offset may be related to pH change in the foraminiferal microenvironment due to symbiont

487 photosynthetic activity (Eggins et al., 2004) or changes in seawater pH, with Mg/Ca of the test
488 increasing by as much as 6±3% for each 0.1 unit decrease in pH (Lea et al., 1999; Russell et al.,
489 2004). pH-related vital effects are reported for other spinose species of planktonic foraminifera
490 such as *Globigerina bulloides* (Lea et al., 1999; Davis et al., 2017), which is related to the genus
491 *Globigerinella* (Fig. 4).

492 Among the neogloboquadrinids, *N. acostaensis* and its descendent *N. humerosa* have the most
493 clearly expressed offset with low Mg/Ca values in the study dataset. In contrast, *Neogloboquadrina*
494 *pachyderma* and *N. incompta* are not offset in the study dataset, perhaps simply because of the
495 limited amount of data (one data point each). More broadly, a Mg/Ca offset compared to other
496 species has been reported in the literature (Davis et al., 2017). *Neogloboquadrina dutertrei*, *N.*
497 *incompta*, *N. pachyderma* and *Pulleniatina obliquiloculata* have been shown to be characterized
498 by much lower trace element concentrations (Mg-Ba-Zn/Ca) in the adult portions of their shells
499 (crust and cortex), so that a greater amount of adult versus early ontogenetic calcite leads to low
500 trace element values in bulk shell analysis (Jonkers et al., 2012; Davis et al., 2017; Fritz-Endres &
501 Fehrenbacher, 2021). The low Mg/Ca of crust and cortex have been found to be independent of
502 ambient temperature in cultured *Neogloboquadrina* (Davis et al., 2017) and are found in specimens
503 collected both in surface waters and at depth (Jonkers et al., 2021), indicating that the low Mg/Ca
504 is not acquired due to calcification in deeper, colder waters of the crust/cortex portion of the shell,
505 although a greater incidence of crusts is reported for colder waters (Jonkers et al., 2021). In our
506 dataset, *Neogloboquadrina*, *Pulleniatina* and *Sphaeroidinella/Sphaerodinellopsis* are all
507 characterized by a thick crust or cortex suggesting their Mg/Ca are biased by low Mg adult calcite
508 being quantitatively predominant, which is further corroborated by their Mg/Ca being unrelated to

509 temperature in our data and consistently falling outside of the $\delta^{18}\text{O}$ -derived temperatures even
510 accounting for the combined uncertainty of the two proxies (Fig. 5 G-H, I-J).

511 The majority of the data points from the offset spinose and non-spinose species results in
512 temperature differences between the two proxies greater than 5°C when using the multi-species
513 calibration from Gray and Evans (2019) as described in §2.4.2, hence outside the calculated error
514 envelope taking all the non-thermal factors discussed above into account (Fig. 5). A similar
515 temperature offset is not apparent for other lineages such *Trilobatus trilobus* – *Trilobatus*
516 *sacculifer* and *Globigerinoides subquadratus* – *G. ruber*, to which the same treatment to the offset
517 spinose and non-spinose species was applied (§2.4.2, Fig. 5 A-D). Hence, we attribute the offset
518 temperatures to the atypical Mg/Ca signatures described above in the affected species, in turn
519 resulting from biology/ecology dependent vital effects shared within a lineage and between related
520 lineages (Figs. 4-5).

521 When a species-specific calibration for *Neogloboquadrina pachyderma* is applied to descendent
522 species/lineages and sister taxa (Fig. 6) the offset is successfully corrected for all the
523 *Neogloboquadrina* and *Pulleniatina* species which effectively no longer produce offset
524 temperatures (Fig. 6). *Vice versa*, we only observe a minor improvement when applying the
525 *Orbulina universa* calibration to the *Pearlobulina-Orbulina* lineage, with most temperature data
526 points remaining offset (Fig. 6). This may imply that the *O. universa* laboratory calibrations require
527 revision for application to fossil samples. No large difference is observed when applying the
528 *Trilobatus sacculifer* calibration to ancestor-descendent species in the genus *Trilobatus* (Figs. 5-
529 7) although we recommend doing so, given that no Mg/Ca-pH effect is known for this genus, in
530 contrast to (e.g.) *G. ruber*.

531 Overall, this exercise demonstrates that the majority of the data points characterized by proxy-
532 proxy disagreement (Fig. 3) are from the lineages: *Praeorbulina-Orbulina*, *Globigerina-*
533 *Globigerinella*, *Neogloquadrina-Pulleniatina*, *Sphaeroidinellopsis-Sphaeroidinella* (Fig. 5). We
534 find that using a “nearest descendant” approach in the choice of temperature calibration improves
535 the agreement between $\delta^{18}\text{O}$ and Mg/Ca temperatures for the neogloboquadrinids and
536 pulleniatinids (Fig. 6). At the same time, it enables us to identify “problematic” species and
537 lineages which require further investigations before being used for temperature reconstructions
538 (Fig. 6). Once all the potential sources of offset described above are taken into account, the species-
539 specific calibration for *Neogloboquadrina* is applied, and the data points which are still offset
540 removed from the dataset, the agreement between the two proxies increased from 62 to 91% of
541 data points falling within the combined uncertainties of the proxies (Fig. 7).

542

543

544

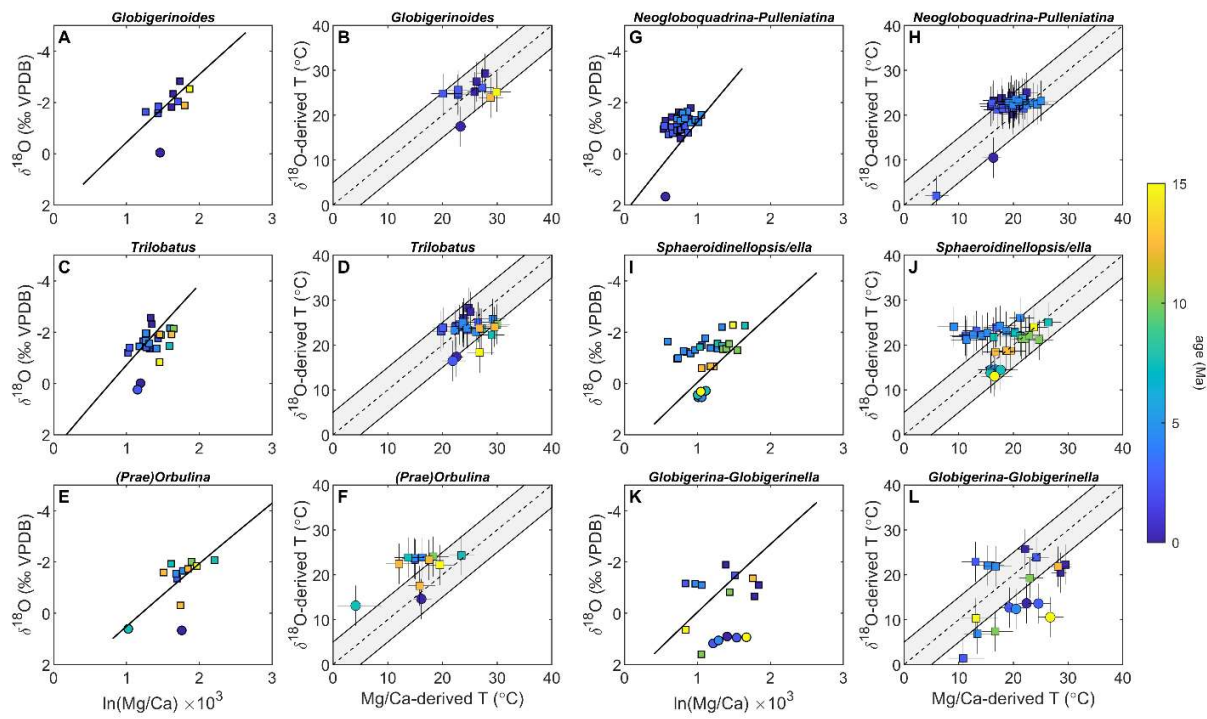
545

546

547

548

549

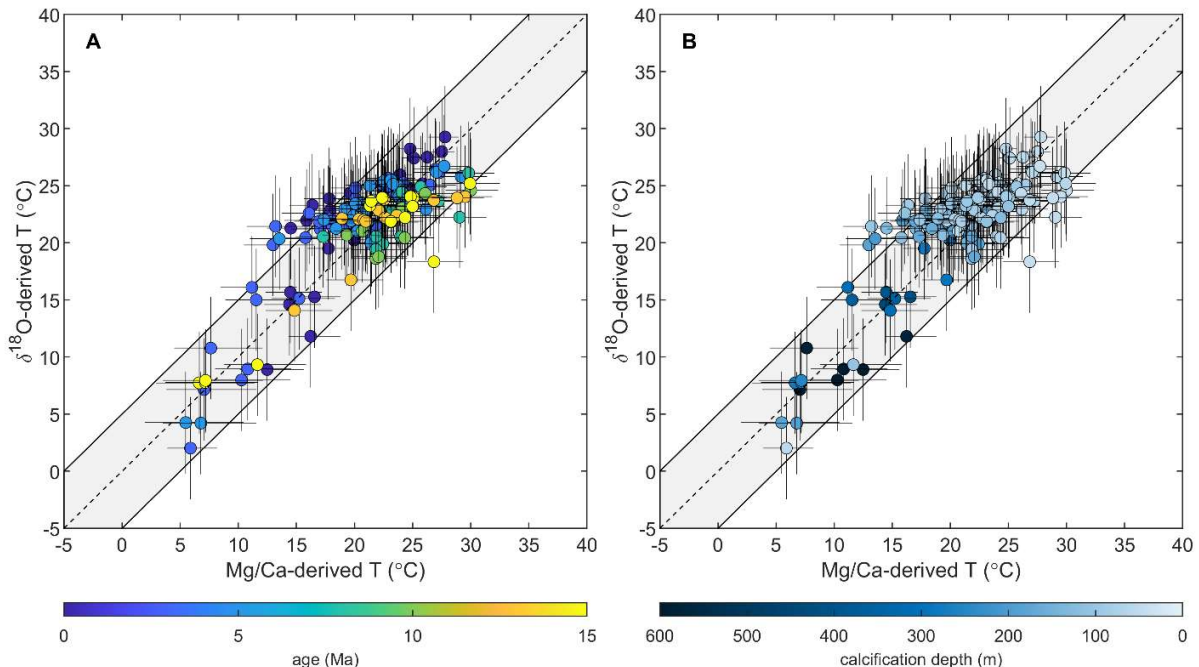


550

551 **Fig. 6.** As in Figure 5, except extending the use of species-specific calibrations to all species in a
 552 lineage in the case of the *Trilobatus trilobus* – *T. sacculifer* (panels C and D), *Praeorbulina*
 553 *glomerosa* – *Orbulina suturalis* – *O. universa* (panels E and F), *Neogloboquadrina acostaensis* –
 554 *N. humerosa*, *N. pachyderma* – *N. incompta*, *N. acostaensis* and between related lineages in the
 555 case of *Neogloboquadrina* and the *Pulleniatina primalis* – *P. praecursor* – *P. finalis* lineage
 556 (panels G and H). When applying species-specific calibrations, the offset between Mg/Ca and $\delta^{18}\text{O}$
 557 temperature is resolved for some species (e.g., all *Neogloboquadrina*, compared to Fig. 5) but not
 558 for others, i.e., their reconstructed temperature still plots outside the gray error envelope (e.g., most
 559 of *Globigerina* and *Globigerinella*).

560

561



562

563 **Fig. 7.** As Fig. 3, with all offset lineages (§ 4.3; specifically, those that remain offset following the
 564 application of lineage-specific calibrations where possible) and diagenetically compromised (§
 565 3.1) samples removed. Removing these samples leaves 157 data points, of which 92% fall within
 566 the combined uncertainty of Mg/Ca- $\delta^{18}\text{O}$ agreement.

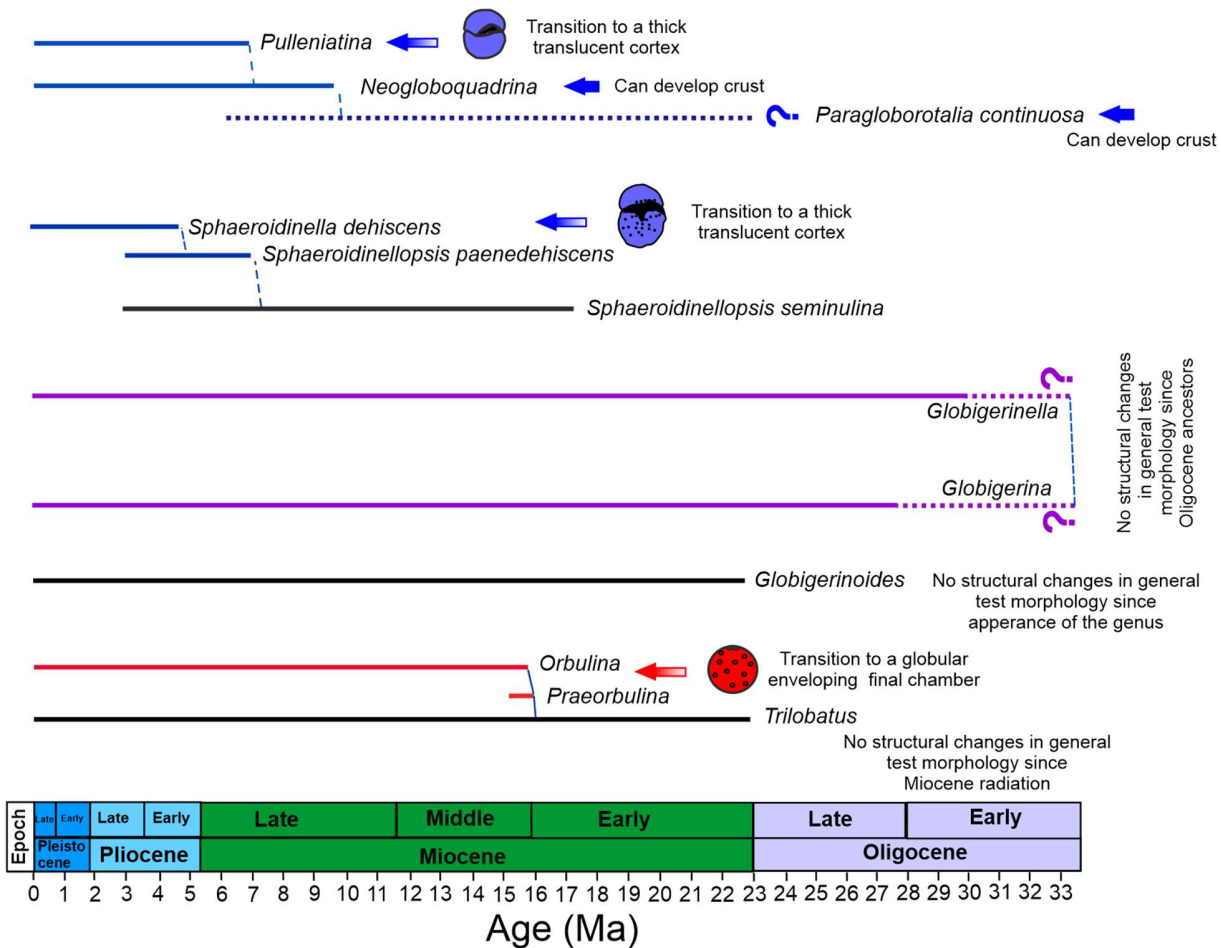
567

568 **4.4. Planktonic foraminiferal Mg/Ca offsets as an expression of evolution**

569 The analysis of the Boscolo-Galazzo, Crichton et al. (2021) dataset performed here, allows offsets
 570 through ancestor-descendent species to be tracked for the first time, and the time of their
 571 appearance to be assessed. Specifically, we observe that offsets tend to appear with the origination
 572 of a new lineage and to continue to the modern representative(s) of that lineage (Fig. 8). In this
 573 way, an attempt can be made to interpret offsets as the geochemical expression of evolutionary
 574 new biochemical pathways or ecological strategies in emerging species.

575 For spinose species, the observed high Mg/Ca offset is shared by ancestor-descendent species such
 576 as *Globigerinella praesiphonifera* - *G. siphonifera* and *Praeorbulina glomerosa* - *Orbulina*

577 *suturalis* - *O. universa* (Fig. 4). *Globigerina bulloides* shares the same type of offset with
578 *Globigerinella* and a common ancestor (*Globigerina archaeobulloides*) in the earliest Oligocene
579 (~33.5 Ma) (Spezzaferri et al., 2018) (Fig. 4), suggesting that for this group the offset may go back
580 to at least the early globigerinids of the Paleogene. The genus *Praeorbulina* originated from the
581 genus *Trilobatus* at about 16 Ma (Fig. 4) (Pearson et al., 1997; Aze et al., 2011). *Trilobatus trilobus*
582 is the last common ancestor between the *Trilobatus* and *Praeorbulina-Orbulina* lineages (Fig. 4),
583 and does not present offset Mg/Ca- $\delta^{18}\text{O}$ values, similar to its modern descendants (Figs. 4, 5). This
584 suggests that the offset in *Praeorbulina-Orbulina* originated within the lineage and the
585 morphological changes associated with it (Fig. 8), and carried on to the modern representative *O.*
586 *universa*. Spinose *Globigerinoides ruber* is also reported to be sensitive to pH changes (Kisakürek
587 et al., 2008; Evans et al., 2016b), *G. ruber* is not offset in the analyzed dataset (both in the raw
588 data and calculated temperatures), with ancestor-descendent *G. subquadratus*-*G. ruber* behaving
589 similarly to the *Trilobatus trilobus* – *T. sacculifer* lineage through time (Figs. 5, 6), suggesting that
590 this non-thermal effect is adequately accounted for in this case (Fig. 6) (i.e., the laboratory
591 calibration are applicable downcore into deep-time in correcting for this). The on-average higher
592 Mg/Ca displayed by offset spinose *Praeorbulina-Orbulina*, *Globigerinella* species and *G.*
593 *bulloides* in the study dataset may suggest a lower pH environment which we cannot directly
594 account for (Fig. 2A). For *Globigerina* and *Globigerinella*, where a larger degree of scatter (Fig.
595 6-7 K-L) is observed in association with a rather conservative morphology through time (Fig. 8),
596 the offset may be linked to an opportunistic behavior and capability to adapt to a broad range of
597 environmental conditions with variable pH (Weiner et al., 2015). This may in turn be related to



612 We find that the low Mg/Ca offset is shared between ancestor-descendent lineages
613 *Neogloboquadrina-Pulleniatina* and *Sphaeroidinellopsis-Sphaerodinella* (Figs. 4, 8).
614 *Neogloboquadrina* evolved from *Paragloborotalia continuosa*, in the late Miocene, at about 10
615 Ma (Fig. 4). While paired Mg/Ca – $\delta^{18}\text{O}$ measurements for *P. continuosa* are not available, paired
616 Mg/Ca – $\delta^{18}\text{O}$ measurements for *Paragloborotalia siakensis*, a species older than *P. continuosa*, do
617 not show a low Mg/Ca offset (Supplementary Table 1). This may indicate either that the occurrence
618 of low Mg/Ca crust/cortex started with *P. continuosa*, the youngest representative of the genus
619 *Paragloborotalia* in our study, or with the neogloboquadrinids. The genus *Pulleniatina* evolved
620 from *Neogloboquadrina acostaensis* at about 6.5 Ma (Pearson et al., 2023) (Fig. 4), by modifying
621 the chambers arrangement and progressively developing a cortex (Fig. 8). *Pulleniatina* may have
622 inherited the capability to thicken its test from *Neogloboquadrina* and modified it into a cortex
623 (Fig. 8) (Pearson et al., 2023). The occurrence of a low Mg/Ca cortex in *Pulleniatina* appears to
624 start from the most ancient representative of this group, *P. primalis* (Fig. 4) and continues to the
625 modern. Similar to *Paragloborotalia*, middle Miocene *Sphaeroidinellopsis kochi* and *S.*
626 *seminulina* are not characterized by an offset to low Mg/Ca values (Figs. 4-6). Nonetheless, an
627 offset is observed in 5 out of 10 specimens for late Miocene – early Pliocene *S. paenedehiscens*,
628 and always occurs for its descendent *Sphaerodinella dehiscens* (Figs. 4-6). Our analysis shows
629 how the occurrence of a low Mg/Ca offset in planktonic foraminifera becomes progressively rarer
630 going back in time, in parallel with the rarity of crust/cortex features (Fig. 8). The occurrence of a
631 crust/cortex is commonly observed in non-spinose modern planktonic foraminifera, however, only
632 two early to middle Miocene genera are known to produce crusts (*Globoconella* and
633 *Paragloborotalia*) and only one is known to produce cortex (*Sphaeroidinellopsis*) (e.g., Fig. 8).

634 It is tempting to put the pattern of emergence of Mg/Ca offsets in relationship with changes in
635 ocean chemistry and global climate over the last 15 Myr. In particular, the offset spinose species
636 are mostly tropical and evolved during a time when mean ocean pH was more than 0.1 pH unit
637 lower than preindustrial (Rae et al., 2021). Further, the *Preorbolina* - *Orbulina* plexus evolved at
638 about 16 Ma (Fig.8), in coincidence with a drop in ocean pH likely linked to the global warmth of
639 the Miocene Climatic Optimum (Rae et al., 2021). The particularly high Mg/Ca signature of this
640 group of species, along with their evolutionary timing, might testify their ability to withstand
641 tropical surface waters more undersaturated than today thanks to changes in the biomineralisation
642 pathway as a consequence of their evolution during the Miocene Climatic Optimum.

643 The evolution of the offset non-spinose species happened several millions of years later during the
644 long-term cooling trend of the last 10 Myr (Fig. 8). The offset species occur across tropical to high
645 latitude areas and mixed-layer (*Sphaeroidinellopsis*, *Sphaeroidinella*) to intermediate
646 (*Neogloboquadrina*, *Pulleniatina*) depth habitats. The ability to develop crust/cortex in species
647 evolving over the last 10 Myr might have been of advantage as the global ocean was becoming
648 progressively colder and denser, in a similar way to the observed increases in shell-mass across
649 Pleistocene glacial cycles (e.g., Zarcogiannis et al., 2019).

650 The last 10 Myr were also characterized by decreasing concentration in Ca_{sw} ($[\text{Ca}^{2+}]$) in step with
651 global cooling, reaching concentrations half those of the middle Miocene in the Recent (Zhou et
652 al., 2021). Partly as a consequence, Mg/Ca_{sw} doubled over the past 15 Ma (Evans et al., 2016b;
653 Rosenthal et al., 2022). With decreasing $[\text{Ca}^{2+}]$ and increasing $[\text{Mg}^{2+}]$ in seawater over the
654 Neogene (Brennan et al., 2013; Evans et al., 2016b; Zhou et al., 2021), some species might have
655 started to more actively control the Mg/Ca ratio at their biomineralisation site, e.g., by
656 proportionally decreasing the active transport of Mg^{2+} , in order to buffer against the effects of the

657 higher seawater Mg/Ca, and to keep the outer parts of their shell with low Mg/Ca and thus more
658 resistant to dissolution. Hence, the low Mg/Ca offset observed in the modern and fossils non-
659 spinose species above might be linked to their evolutionary emergence during a time of changing
660 ocean physical-chemical properties, which may have promoted the evolution of thicker tests with
661 a different elemental chemistry making them less buoyant and resistant to dissolution.

662 **5. Conclusions**

663 We analyzed a multispecies planktonic foraminiferal $\delta^{18}\text{O}$ and Mg/Ca dataset spanning the last 15
664 million years at multiple locations to test whether temperature is the main controller of both proxies
665 and assess the major overprinting factors through time, space and for species with very distinct
666 ecologies. Once diagenesis and possible regional hydrographic factors are taken into account, we
667 find that species-specific offsets not accounted for in our calibration strategy remain a source of
668 mismatch between the two proxies. Specifically, *Globigerina*, *Globigerinella*, *Praeorbulina* and
669 *Orbulina* species are consistently offset, with Mg/Ca values on average higher than expected.
670 Conversely, non-spinose *Neogloboquadrina*, *Pulleniatina*, *Sphaeroidinellpsis* and
671 *Sphaeroidinella* appear consistently offset with low Mg/Ca. The appearance of these geochemical
672 offsets appears to be linked to the origination of new clades, and is shared between ancestor-
673 descendent species, such that we were able to track their evolutionary history. The variable offset
674 in *Globigerinella* may go back to the early globigerinids of the Paleogene and could be related to
675 the opportunistic behavior of this group and emergence of multiple genotypes through geological
676 time, leading to a wider-range of habitat conditions. The high Mg/Ca offset in *Orbulina* starts with
677 *Praeorbulina* in the middle Miocene, while a low Mg/Ca offset appears typical of groups evolving
678 in the late Neogene characterized by a crust or cortex. This pattern suggests that the offsets

679 observed in modern species may be a legacy of their parent groups originating millions of years
680 ago, when ocean properties were different from today.

681 Overall, our study highlights the power of the multispecies and multi-time slice dataset presented
682 here, enabling us to identify the evolutionary origin and timing of deviations in Mg/Ca-
683 temperature/pH relationships. Furthermore, our study demonstrates the robustness of Mg/Ca and
684 $\delta^{18}\text{O}$ proxies through geologic time when nonthermal factors (especially Mg/Ca_{sw} and pH) are
685 accounted for. For example, virtually all *Globigerinoides* and *Trilobatus* Mg/Ca and $\delta^{18}\text{O}$ -derived
686 temperatures are within uncertainty of each other, highlighting the utility of these species for
687 paleoceanographic reconstruction. In addition, our analysis enables us to identify species/lineages
688 that should be treated with caution when interpreting Mg/Ca data, at the very least demonstrating
689 that care should be taken in selecting the calibration approach and highlighting the need for further
690 work in understanding the nonthermal controls on Mg incorporation into the shells of these
691 foraminifera.

692 **Code and Data availability**

693 All data are available as supplementary material of this paper. R and Matlab code to perform the
694 ‘MgCaRB’ protocols are available on Github: <https://github.com/willyrgray/> MgCaRB for R,
695 <https://github.com/dbjewans/MgCaRB/releases/tag/v1.3> for Matlab. The code to perform the
696 calculations and produce the figures is available at: DOI: 10.5281/zenodo.14348660.

697 **Author contributions**

698 E.M.M. performed trace element analysis; F.B.G conceptualized the paper; D.E. performed data
699 analysis; F.B.G and D.E. produced the figures; F.B.G and D.E. wrote the paper with contributions
700 from all authors.

701 **Competing interests**

702 The authors declare no competing interests.

703 **Acknowledgments**

704 This study was funded by Natural Environment Research Council (NERC) grant NE/N001621/1
705 to P.N.P. (F.B.G.); NERC grant NE/P016375/1 to participate in IODP Expedition 363 (P.N.P.);
706 and NERC grant NE/N002598/1 to B.S.W. (E.M.M.). Marcin Latas assisted with sample
707 preparation funded by an EU Marie Curie Career Integration Grant 293741 to B.S.W; F.B.G
708 acknowledges support from Horizon 2020 Framework Programme (H2020-MSCA-IF-2020
709 101019438).

710 **References**

- 711 1. Anand, P., Elderfield, H., and Conte, M.H.: Calibration of Mg/Ca thermometry in
712 planktonic foraminifera from a sediment trap time series, *Paleoceanography* 18, 1050,
713 10.1029/2002PA000846, 2003.
- 714 2. Aze, T., Ezard, T.H.G., Purvis, A., Coxall, H.K., Stewart, D.R.M., Wade, B.S., and
715 Pearson, P.N.: A phylogeny of Cenozoic macroperforate planktonic foraminifera from
716 fossil data, *Biological Reviews* 86, 900–927, 10.1111/j.1469-185X.2011.00178, 2011.
- 717 3. Barker, S., Greaves, M., and Elderfield, H.: A study of cleaning procedures used for
718 foraminiferal Mg/Ca paleothermometry, *Geochemistry, Geophysics, Geosystems* 4,
719 10.1029/2003GC000559, 2003.
- 720 4. Birch, H., Coxall, H.K., Pearson, P.N., Kroon, D., and O'Regan, M.: Planktonic
721 foraminifera stable isotopes and water column structure: Disentangling ecological signals,
722 *Marine Micropaleontology* 10, 127–145, 10.1016/j.marmicro.2013.02.002, 2013.

723 5. Boscolo-Galazzo, F., Crichton, K.A., Ridgwell, A., Mawbey, E.M., Wade, B.S., and
724 Pearson P.N.: Temperature controls carbon cycling and biological evolution in the ocean
725 twilight zone, *Science*, 371, 1148–1152, 10.1126/science.abb6643, 2021.

726 6. Boscolo-Galazzo, F., Jones, A., Dunkley Jones, T., Crichton, K.A., Wade, B.S., and
727 Pearson, P.N.: Late Neogene evolution of modern deep-dwelling plankton,
728 *Biogeosciences*, 19, 743-762, doi.org/10.5194/bg-19-743-2022, 2022.

729 7. Branson, O., Read, E., Redfern, S. A. T., Rau, C., and Elderfield, H.: Revisiting diagenesis
730 on the Ontong Java Plateau: Evidence for authigenic crust precipitation in *Globorotalia*
731 *tumida*, *Paleoceanography* 30, 1490–1502, 10.1002/2014PA002759, 2015.

732 8. Brennan, S.T., Lowenstein, T.K., and Cendon, D.I.: The major-ion composition of
733 Cenozoic seawater: the past 36 million years from fluid inclusions in marine halite,
734 *American Journal of Science* 313, 713–775, doi.org/10.2475/08.2013.01, 2013.

735 9. Burke, K.D., Williams, J.W., Chandler, M.A., Haywood, A.M., Lunt, D.J., and Otto-
736 Bliesner, B.L.: Pliocene and Eocene provide best analogs for near-future climates,
737 *Proceedings of the National Academy of Sciences* 115, 13288-13293,
738 doi.org/10.1073/pnas.1809600115, 2018.

739 10. Chave, K. E.: Aspects of the biogeochemistry of magnesium 1. Calcareous marine
740 organisms, *The Journal of Geology*, 62, 266-283, 10.1086/626162, 1954.

741 11. Daëron, M., and Gray, W. R. Revisiting oxygen-18 and clumped isotopes in planktic and
742 benthic foraminifera. *Paleoceanography and Paleoceanography*, 38, e2023PA004660, 2023.

743 12. Davis, C.V., Fehrenbacher, J.S., Hill, T.M., Russell, A.D., and Spero, H.J.: Relationships
744 between temperature, pH, and crusting on Mg/Ca ratios in laboratory-grown

745 Neogloboquadrina foraminifera, Paleoceanography 32, 2017PA003111,
746 10.1002/2017PA003111, 2017.

747 13. Dekens, P.S., Lea, D.W., Pak, D.K., and Spero, H.J.: Core top calibration of Mg/Ca in
748 tropical foraminifera: Refining paleotemperature estimation, *Geochemistry, Geophysics,
749 Geosystems* 3, 1-29, 10.1029/2001GC000200, 2002.

750 14. Edgar, K.M., Anagnostou, E., Pearson, P.N., and Foster, G.L.: Assessing the impact of
751 diagenesis on $\delta^{11}\text{B}$, $\delta^{13}\text{C}$, $\delta^{18}\text{O}$, Sr/Ca and B/Ca values in fossil planktic foraminiferal
752 calcite, *Geochimica et Cosmochimica Acta* 166, 189–209, 10.1016/j.gca.2015.06.018,
753 2015.

754 15. Eggins S. M., Sadekov A. and De Deckker P.: Modulation and daily banding of Mg/Ca in
755 *Orbulina universa* tests by symbiont photosynthesis and respiration: a complication for
756 seawater thermometry? *Earth Planetary Science Letters* 225, 411–419,
757 10.1016/j.epsl.2004.06.019, 2004.

758 16. Elderfield, H., and Ganssen, G.: Past temperature and $\delta^{18}\text{O}$ of surface ocean waters
759 inferred from foraminiferal Mg/Ca ratios, *Nature* 405, 442, 10.1038/35013033, 2004.

760 17. Elderfield, H., Yu, J., Anand, P., Kiefer, T., and Nyland, B.: Calibrations for benthic
761 foraminiferal Mg/Ca paleothermometry and the carbonate ion hypothesis, *Earth and
762 Planetary Science Letters* 250, 633-649, 10.1016/j.epsl.2006.07.041, 2006.

763 18. Emiliani, C.: Depth habitats of some species of pelagic foraminifera as indicated by oxygen
764 isotope ratios, *American Journal of Science* 252, 149-158, 1954.

765 19. Erez, J., and Luz, B.: Experimental paleotemperature equation for planktonic foraminifera,
766 *Geochimica et Cosmochimica Acta* 47, 1025 – 1031, 10.1016/0016-7037(83)90232-6,
767 1983.

768 20. Evans D., Erez J., Oron S. and Muller W.: Mg/Ca temperature and seawater-test chemistry
769 relationships in the shallow-dwelling large benthic foraminifera *Operculina ammonoides*,
770 *Geochimica and Cosmochimica Acta* 148, 325–342, 10.1016/j.gca.2014.09.039, 2015.

771 21. Evans, D., Wade, B.S., Henehan, M., Erez, J., and Müller, W.: Revisiting carbonate
772 chemistry controls on planktic foraminifera Mg/Ca: Implications for sea surface
773 temperature and hydrology shifts over the Paleocene-Eocene Thermal Maximum and
774 Eocene-Oligocene transition, *Climate of the Past* 12, 819–835, 10.5194/cp-12-819-2016,
775 2016a.

776 22. Evans, D., Brierley, C., Raymo, M.E., Erez, J., and Müller, W.: Planktic foraminifera shell
777 chemistry response to seawater chemistry: Pliocene–Pleistocene seawater Mg/Ca,
778 temperature and sea level change, *Earth and Planetary Science Letters* 438, 139-148,
779 2016b, 10.1016/j.epsl.2016.01.013.

780 23. Fabbrini, A., Zaminga, I., Ezard, T. and Wade, B.S.: Systematic taxonomy of middle
781 Miocene *Sphaeroidinellopsis* (planktonic foraminifera), *Journal of Systematic*
782 *Palaeontology*, 19, 953-968, 10.1080/14772019.2021.1991500, 2021.

783 24. Fayolle, F. and Wade, B.S.: Data report: Miocene planktonic foraminifers
784 *Dentoglobigerina* and *Globoquadrina* from IODP Sites U1489 and U1490, Expedition
785 363. In: Rosenthal, Y., Holbourn, A.E., Kulhanek, D.K., and the Expedition 363 Scientists,
786 Western Pacific Warm Pool. *Proceedings of the International Ocean Discovery Program*,
787 363: College Station, TX (International Ocean Discovery Program),
788 10.14379/iodp.proc.363.203.2020, 2020.

789 25. Friedrich, O., Schiebel, R., Wilson, P.A., Weldeab, S., Beer, C.J., Cooper, M.J., and Fiebig,
790 J.: Influence of test size, water depth, and ecology on Mg/Ca, Sr/Ca, $\delta^{18}\text{O}$ and $\delta^{13}\text{C}$ in

791 nine modern species of planktic foraminifers, *Earth and Planetary Science Letters* 319,
792 133–145, 10.1016/j.epsl.2011.12.002, 2012.

793 26. Fritz-Endres, T., and Fehrenbacher, J.: Preferential loss of high trace element bearing inner
794 calcite in foraminifera during physical and chemical cleaning, *Geochemistry, Geophysics,
795 Geosystems*, 22, e2020GC009419, 10.1029/2020GC009419, 2021.

796 27. Gaskell, D.E., and Hull, P.: Technical note: A new online tool for $\delta^{18}\text{O}$ –temperature
797 conversions, *Climate of the past* 19, 1265–1274, 10.5194/cp-19-1265-2023, 2023.

798 28. Gaskell, D.E., Huber, M., O’Brien, C.L., Inglis, G.N., Acosta, R.P., Poulsen, C.J., and Hull,
799 P.M.: The latitudinal temperature gradient and its climate dependence as inferred from
800 foraminiferal ^{18}O over the past 95 million years, *Proceedings of the National Academy of
801 Science USA* 119, e2111332119, 10.1073/pnas.2111332119, 2022.

802 29. Gray, W.R., and Evans, D.: Nonthermal influences on Mg/Ca in planktonic foraminifera:
803 A review of culture studies and application to the last glacial maximum, *Paleoceanography
804 and Paleoclimatology* 34, 306–315, 10.1029/2018PA003517, 2019.

805 30. Gray, W. R., Weldeab, S., Lea, D. W., Rosenthal, Y., Gruber, N., Donner, B., and Fischer,
806 G.: The effects of temperature, salinity, and the carbonate system on Mg/Ca in
807 *Globigerinoides ruber* (white): A global sediment trap calibration, *Earth and Planetary
808 Science Letters* 482, 607–620, 10.1016/j.epsl.2017.11.026, 2018.

809 31. Holland, K., Branson, O., Haynes, L.L., Honisch, B., Allen, K.A., Russell, A.D.,
810 Fehrenbacher, J.S., Spero, H.J., and Eggins S.M.: Constraining multiple controls on
811 planktic foraminifera Mg/Ca, *Geochimica et Cosmochimica Acta* 273, 116–136,
812 10.1016/j.gca.2020.01.015, 2020.

813 32. Hönisch, B., Allen, K.A., Lea, D.W., Spero, H.J., Eggins, S.M., Arbuszewski, J., deMenocal, P., Rosenthal, Y., Russell, A.D., and Elderfield, H.: The influence of salinity on Mg/Ca
814 in planktic foraminifers – evidence from cultures, core-top sediments and complementary
815 $\delta^{18}\text{O}$, *Geochim. Cosmochim. Acta* 121, 196–213, 10.1016/j.gca.2013.07.028, 2013.

816

817 33. Huber, B.T., Petrizzo, M.R., Young, J., Falzoni, F., Gilardoni, S., Bown, P.R., and Wade,
818 B.S.: Pforams@mikrotax: A new online taxonomic database for planktonic foraminifera,
819 *Micropalaeontology*, 62: 429-438, 2016.

820

821 34. John, E.H., Staudigel, P.T., Buse, B., Lear, C.H., Pearson, P.N., and Slater, S.M.: Revealing
822 their true stripes: Mg/Ca banding in the Paleogene planktonic foraminifera genus
823 *Morozovella* and implications for paleothermometry, Paleoceanography and
824 Paleoclimatology, 38, e2023PA004652, 10.1029/2023PA004652, 2023.

825

826 35. Jonkers, L., de Nooijer, L.J., Reichart, G.-J., Zahn, R., and Brummer, G.-J.A.: Encrustation
827 and trace element composition of *Neogloboquadrina dutertrei* assessed from single
828 chamber analyses – implications for paleotemperature estimates, *Biogeosciences*, 9, 4851–
829 4860, 10.5194/bg-9-4851-2012, 2012.

830

831 36. Jonkers, L., Gopalakrishnan, A., Weßel, L., Chiessi, C. M., Groeneveld, J., Monien, P., et
832 al.: Morphotype and crust effects on the geochemistry of *Globorotalia inflata*,
833 Paleoceanography and Paleoclimatology 36, e2021PA004224, 10.1029/2021PA004224 ,
834 2021.

835

836 37. Kisakürek, B., Eisenhauer, A., Böhm, F., Garbe-Schönberg, D., and Erez, J.: Controls on
837 shell Mg/Ca and Sr/Ca in cultured planktonic foraminiferan, *Globigerinoides ruber*
838 (white), *Earth and Planetary Science Letters* 273, 260-269, 10.1016/j.epsl.2008.06.026,
839 2008.

836 38. LeGrande A.N., and Schmidt G.A.: Global gridded data set of the oxygen isotopic
837 composition in seawater, *Geophys. Res. Lett.* 33, L12604, 10.1029/2006GL026011, 2006.

838 39. Lea, D.W., Mashiotta, T.A., and Spero, H.J.: Controls on magnesium and strontium uptake
839 in planktonic foraminifera determined by live culturing, *Geochimica et Cosmochimica
840 Acta* 63, 2369-2379, 10.1016/S0016-7037(99)00197-0, 1999.

841 40. Lear, C.H., Rosenthal, Y., and Slowey, N.: Benthic foraminiferal Mg/Ca-
842 paleothermometry: A revised core-top calibration, *Geochimica et Cosmochimica Acta* 66,
843 3375-3387, 10.1016/S0016-7037(02)00941-9, 2002.

844 41. Leckie, R.M., Wade, B.S., Pearson, P.N., Fraass, A.J., King, D.J., Olsson, R.K., Premoli
845 Silva, I., Spezzaferri, S., and Berggren, W.A.: Taxonomy, biostratigraphy, and phylogeny
846 of Oligocene and early Miocene *Paragloborotalia* and *Parasubbotina*, in Wade, B.S.,
847 Olsson, R.K., Pearson, P.N., Huber, B.T. and Berggren, W.A., *Atlas of Oligocene
848 Planktonic Foraminifera*, Cushman Foundation of Foraminiferal Research, Special
849 Publication, No. 46, p. 125-178, 2018.

850 42. Locarnini, R. A., Mishonov, A.V., Antonov, J.I., Boyer, T.P., Garcia, H.E., Baranova,
851 O.K., Zweng, M.M., Paver, C.R., Reagan, J.R., Johnson, D.R., Hamilton, M., and Seidov,
852 D.: *World Ocean Atlas 2013, Volume 1: Temperature*. S. Levitus, Ed., A. Mishonov
853 Technical Ed.; NOAA Atlas NESDIS 73, 40 pp, 2013.

854 43. Lourens, L.J., Hilgen, F.J., Shackleton, N.J., Laskar, J., and Wilson, D.: The Neogene
855 Period. In: Gradstein, F.M., Ogg, J.G., Smith, A.G. (Eds.), *Geological Time Scale 2004*.
856 Cambridge University Press, pp. 409–440, 2004.

857 44. Malevich, S. B., Vetter, L., and Tierney, J. E.: Global Core Top Calibration of ^{18}O in
858 Planktic Foraminifera to Sea Surface Temperature, *Paleoceanography* and
859 *Paleoclimatology*, 34, 1292–1315, 10.1029/2019PA003576, 2019.

860 45. Mathien-Blard, E., and Bassinot, F.: Salinity bias on the foraminifera Mg/Ca thermometry:
861 correction procedure and implications for past ocean hydrographic reconstructions,
862 *Geochem. Geophys. Geosyst.* 10, Q12011, 10.1029/2008GC002353, 2009.

863 46. McConnell, M.C., and Thunell, R.C.: Calibration of the planktonic foraminiferal Mg/Ca
864 paleothermometer: sediment trap results from the Guaymas Basin, Gulf of California.
865 *Paleoceanography* 20, PA2016, 10.1029/2004PA001077, 2005.

866 47. Miller, K.G., Kominz, M.A., Browning, J.V., Wright, J.D., Mountain, G.S., Katz, M.E.,
867 Sugarman, P.J., Cramer, B.S., Christie-Blick, N., and Pekar, S.F.: The Phanerozoic record
868 of global sea-level change, *Science* 310, 1293–1298, 10.1126/science.1116412, 2005.

869 48. Miller, K.G., Browning, J.V., Schmelz, W.J., Kopp, R.E., Mountain, G.S., Wright, J.D.:
870 Cenozoic sea-level and cryospheric evolution from deep-sea geochemical and continental
871 margin records, *Science Advances* 6, eaaz1346, 2020.

872 49. Morard, R., Darling, K.F., Weiner, A.K.M., Hassenrück, C., Vanni, C., Cordier, T., Henry,
873 N., Greco, M., Vollma, N.M., Milivojevic, T., Rahman, S.N., Siccha, M., Meiland, J.,
874 Jonkers, L., Quillévéré, F., Escarguel, G., Douady, C.J., de Garidel-Thoron, T., de Vargas,
875 C., and Kucera, M.: The global genetic diversity of planktonic foraminifera reveals the
876 structure of cryptic speciation in plankton, *Biological Reviews*, 10.1111/brv.13065, 2024.

877 50. Mucci, A.: Influence of temperature on the composition of magnesian calcite overgrowths
878 precipitated from seawater, *Geochimica et Cosmochimica Acta* 51, 1977-1984,
879 10.1016/0016-7037(87)90186-4, 1987.

880 51. Mucci, A., Morse, J.W.: The incorporation of Mg²⁺ and Sr²⁺ into calcite overgrowths:
881 influences of growth rate and solution composition, *Geochimica et Cosmochimica Acta*
882 47, 217-233, 10.1016/0016-7037(83)90135-7, 1983.

883 52. Nuernberg, D.: Magnesium in tests of *Neogloboquadrina pachyderma* sinistral from high
884 northern and southern latitudes, *The Journal of Foraminiferal Research* 25, 350-368,
885 10.2113/gsjfr.25.4.350, 1995.

886 53. Nürnberg, D., Bijma, J., and Hemleben, C.: Assessing the reliability of magnesium in
887 foraminiferal calcite as a proxy for water mass temperatures, *Geochimica et Cosmochimica
888 Acta* 60, 803-814, 10.1016/0016-7037(95)00446-7, 1996.

889 54. Opdyke, B.N., and Pearson, P.N.: Data report: geochemical analysis of multiple planktonic
890 foraminifer species at discrete time intervals, In: Haggerty, J.A., Premoli Silva, I., Rack,
891 F., and McNutt, M.K. (Eds.), *Proceedings of the Ocean Drilling Program, Scientific
892 Results*, 144, 993-995, 10.2973/odp.proc.sr.144.052.1995, 1995.

893 55. Pälike, H., Norris, R.D., Herrle, J.O., Wilson, P.A., Coxall, H.K., and Lear, C.H.,
894 Shackleton, N.J., Tripati, A.K., Wade, B.S.: The heartbeat of the Oligocene climate system,
895 *Science* 314, 1894–1898, 10.1126/science.1133822, 2006.

896 56. Pearson, P.N., Shackleton, N.J., and Hall, M.A.: Stable isotopic evidence for the sympatric
897 divergence of *Globigerinoides trilobus* and *Orbulina universa*, *Journal of the Geological
898 Society*, 154, 295–302, 10.1144/gsjgs.154.2.0295, 1997.

899 57. Pearson, P.N.: Oxygen isotopes in foraminifera: overview and historical review. In
900 *Reconstructing Earth's Deep-Time Climate*, *Paleontological Society Papers* Volume 18, L.
901 Ivany, B. Huber, Eds. (2012), pp. 1–38, 2012.

902 58. Pearson, P.N., Young, J., King, D.J., and Wade, B.S.: Biochronology and evolution of
903 *Pulleniatina* (planktonic foraminifera), *Journal of Micropalaeontology*, 42, 211–255,
904 10.5194/jm-42-211-2023, 2023.

905 59. Rae, J.W.B., Zhang, Y., Liu, X., Foster, G.L., Stoll, H.M., and Whiteford, D.M.:
906 Atmospheric CO₂ over the past 66 million years from marine archives, *Annual Review of*
907 *Earth and Planetary Sciences* 49, 609–641, 10.1146/annurev-earth-082420-063026, 2021.

908 60. Regenberg, M., Regenberg, A., Garbe-Schönberg, D., and Lea, D.W.: Global dissolution
909 effects on planktonic foraminiferal Mg/Ca ratios controlled by the calcite-saturation state
910 of bottom waters, *Paleoceanography*, 29, 127–142, 10.1002/2013PA002492, 2014.

911 61. Rohling, E. J., Foster, G. L., Gernon, T. M., Grant, K. M., Heslop, D., Hibbert, F. D., et
912 al.: Comparison and synthesis of sea-level and deep-sea temperature variations over the
913 past 40 million years. *Reviews of Geophysics*, 60, e2022RG000775, 2022.

914 62. Rongstad, B.L., Marchitto, T.M., and Herguera, J.C.: Understanding the effects of
915 dissolution on the Mg/Ca paleothermometer in planktic foraminifera: Evidence from a
916 novel individual foraminifera method, *Paleoceanography* 32, 1386–1402,
917 10.1002/2017PA003179, 2017.

918 63. Rosenthal, Y., Bova, S., and Zhou, X.: A user guide for choosing planktic foraminiferal
919 Mg/Ca-temperature calibrations. *Paleoceanography and Paleoclimatology* 37,
920 e2022PA004413, 2022.

921 64. Russell, A.D., Honisch, B., Spero, H.J., Lea, D.W.: Effects of seawater carbonate ion
922 concentration and temperature on shell U, Mg, and Sr in cultured planktonic foraminifera,
923 *Geochimica and Cosmochimica Acta* 68, 4347–4361, 10.1016/j.gca.2004.03.013, 2004.

924 65. Sexton, P.E., Wilson, P.A., and Pearson, P.N.: Microstructural and geochemical
925 perspectives on planktic foraminiferal preservation: “Glassy” versus “Frosty”, *Geochem.*
926 *Geophys. Geosyst.* 7, 10.1029/2006GC001291, 2006.

927 66. Schiebel, R., and Hemleben, C.: *Planktic foraminifers in the modern ocean*. Springer, 2017.

928 67. Spero, H.J., Bijma, J., Lea, D.W., Bemis, B.E.: Effect of seawater carbonate concentration
929 on foraminiferal carbon and oxygen isotopes, *Nature* 390, 497-500, 10.1038/37333, 1997.

930 68. Spezzaferri, S., Coxall, H.K., Olsson, R.K., and Hemleben, C.: Taxonomy, biostratigraphy
931 and phylogeny of Oligocene *Globigerina*, *Globigerinella*, and *Quiltyella* n. gen., in Wade,
932 B.S., Olsson, R.K., Pearson, P.N., Huber, B.T. and Berggren, W.A., *Atlas of Oligocene*
933 *Planktonic Foraminifera*, Cushman Foundation of Foraminiferal Research, Special
934 Publication, No. 46, p. 125-178, 2018.

935 69. Spratt, R.M., and Lisiecki, L.: A Late Pleistocene sea-level stack, *Climate of the past* 12,
936 1070-1092, 10.5194/cp-12-1079-2016, 2016.

937 70. Staudigel, P.T., John, E.H., Buse, B., Pearson, P.N., and Lear, C.H.: Apparent preservation
938 of primary foraminiferal Mg/Ca ratios and Mg-banding in recrystallized foraminifera,
939 *Geology* 50, 760–764, 10.1130/G49984.1, 2022.

940 71. Tierney, J.E., Malevich, S.B., Gray, W., Vetter, L., and Thirumalai, K.: Bayesian
941 calibration of the Mg/Ca paleothermometer in planktic foraminifera, *Paleoceanography*
942 and *Paleoclimatology* 34, 2005-2030, 10.1029/2019PA003744, 2019.

943 72. Urey, H.C.: The thermodynamic properties of isotopic substance, *Journal of the Chemical*
944 *Society of London* 1947, 562–581, 1947.

945 73. Urey, H.C. Oxygen isotopes in nature and in the laboratory, *Science* 108, 489–496, 1948.

946 74. Von Langen, P.J., Pak, D.K., Spero, H.J., and Lea, D.W.: Effects of temperature on Mg/Ca
947 in neogloboquadrinid shells determined by live culturing, *Geochemistry, Geophysics,
948 Geosystems* 6, 10.1029/2005GC000989, 2005.

949 75. Wade, B.S., Pearson, P.N., Berggren, W.A., and Pälike, H.: Review and revision of
950 Cenozoic tropical planktonic foraminiferal biostratigraphy and calibration to the
951 geomagnetic polarity and astronomical time scale, *Earth-Science Reviews* 104, 111-142,
952 10.1016/j.earscirev.2010.09.003, 2011.

953 76. Weiner, A.K.M., Weinkauf, M.F.G., Kurasawa, A., Darling, K.F., and Kucera, M.: Genetic
954 and morphometric evidence for parallel evolution of the *Globigerinella calida*
955 morphotype, *Marine Micropaleontology* 114, 19–35, 10.1016/j.marmicro.2014.10.003,
956 2015.

957 77. Westerhold, T., Marwan, N., Drury, A.J., Liebrand, D., Agnini, C., Anagnostou, E., Barnet,
958 J.S.K., Bohaty, S.M., Vleeschouwer, D.D., Florindo, F., Frederichs, T., Hodell, D.A.,
959 Holbourn, A. E., Kroon, D., Lauretano, V., Littler, K., Lourens, L.J., Lyle, M., Pälike, H.,
960 Röhl, U., Tian, J., Wilkens, R.H., Wilson, P.A., and Zachos, J.C.: Anastronomically dated
961 record of Earth's climate and its predictability over the last 66 million years, *Science*, 369,
962 1383–1387, 10.1126/science.aba6853, 2020.

963 78. Yu, J., Elderfield, H., Greaves, M., and Day, J.: Preferential dissolution of benthic
964 foraminiferal calcite during laboratory reductive cleaning, *Geochemistry, Geophysics,
965 Geosystems* 8, 10.1029/2006GC001571, 2007.

966 79. Zarkogiannis, S.D., Antonarakou, A., Tripati, A., Kontakiotis, G., Mortyn, P.G., Drinia,
967 H., and Greaves, M.: Influence of surface ocean density on planktonic foraminifera
968 calcification, *Scientific Reports* 9, 10.1038/s41598-018-36935-7, 2019.

969 80. Zeebe, R. E.: An explanation of the effect of sea water carbonate concentration on
970 foraminiferal oxygen isotopes, *Geochimica, Cosmochimica, Acta* 63, 2001–2007,
971 10.1016/S0016-7037(99)00091-5, 1999.

972 81. Zeebe, R.E., and Tyrrell, T.: History of carbonate ion concentration over the last 100
973 million years II: revised calculations and new data, *Geochimica and Cosmochimica Acta*
974 257, 373–392, 10.1016/j.gca.2019.02.041, 2019.

975 82. Zhou, X., Rosenthal, Y., Haynes, L., Si W., Evans, D., Huang, K.-F., Honisch, B., and
976 Erez, J.: Planktic foraminiferal Na/Ca: A potential proxy for seawater calcium
977 concentration, *Geochimica et Cosmochimica Acta* 305, 306–322,
978 10.1016/j.gca.2021.04.012, 2021.